

Genome-scale metabolic modelling of responses to polymyxins in *Pseudomonas aeruginosa* --Manuscript Draft--

Manuscript Number:	GIGA-D-17-00272	
Full Title:	Genome-scale metabolic modelling of responses to polymyxins in <i>Pseudomonas aeruginosa</i>	
Article Type:	Research	
Funding Information:	Monash University (Major Interdisciplinary Research Grant)	Prof Jian Li
	National Health and Medical Research Council (APP1127948)	Prof Jian Li
	National Institute of Allergy and Infectious Diseases (R01 AI111965)	Prof Jian Li
	National Health and Medical Research Council (APP1086825)	Dr Tony Velkov
	National Health and Medical Research Council (APP1063069)	Prof Jian Li
	Australian Research Council (FL130100038)	Prof Trevor Lithgow
Abstract:	<p>Background: <i>Pseudomonas aeruginosa</i> often causes multidrug-resistant infections in immunocompromised patients and polymyxins are often used as the last-line therapy. Alarming, resistance to polymyxins has been increasingly reported worldwide recently. To rescue this last-resort class of antibiotics, it is necessary to systematically understand how <i>P. aeruginosa</i> alters its metabolism in response to polymyxin treatment, thereby facilitating the development of effective antimicrobial therapies. To this end, genome-scale metabolic model (GSMM) was employed to analyse bacterial metabolic changes at the systems level.</p> <p>Findings: A high-quality GSMM iPAO1 was constructed for <i>P. aeruginosa</i> PAO1 for antimicrobial pharmacological research. Model iPAO1 encompasses an additional periplasmic compartment and contains 3,022 metabolites, 4,265 reactions and 1,458 genes in total. Growth prediction on 190 carbon and 95 nitrogen sources achieved an accuracy of 89.1%, outperforming all reported <i>P. aeruginosa</i> models. Notably, prediction of the essential genes for growth achieved a high accuracy of 87.9%. Metabolic simulation showed that lipid A modifications associated with polymyxin resistance exert a limited impact on bacterial growth and metabolism, but remarkably change the physiochemical properties of the outer membrane. Modelling with transcriptomics constraints revealed a broad range of metabolic responses to polymyxin treatment, including reduced biomass synthesis, upregulated amino acids catabolism, induced flux through the tricarboxylic acid cycle, and increased redox turnover.</p> <p>Conclusions: Overall, iPAO1 represents the most comprehensive GSMM constructed to date for a Gram-negative bacterium. It provides a powerful systems pharmacology platform for the elucidation of complex killing mechanisms of antibiotics.</p>	
Corresponding Author:	Jian Li AUSTRALIA	
Corresponding Author Secondary Information:		
Corresponding Author's Institution:		
Corresponding Author's Secondary Institution:		
First Author:	Yan Zhu	

First Author Secondary Information:	
Order of Authors:	Yan Zhu
	Tobias Czauderna
	Jinxin Zhao
	Matthias Klapperstueck
	Mohd Hafidz Mahamad Maifiah
	Mei-Ling Han
	Jing Lu
	Björn Sommer
	Tony Velkov
	Trevor Lithgow
	Jiangning Song
	Falk Schreiber
	Jian Li
Order of Authors Secondary Information:	
Opposed Reviewers:	Jason Papin, Ph.D. Professor of Biomedical Engineering, University of Virginia papin@virginia.edu Conflicts of research
Additional Information:	
Question	Response
Are you submitting this manuscript to a special series or article collection?	No
Experimental design and statistics	Yes
Full details of the experimental design and statistical methods used should be given in the Methods section, as detailed in our Minimum Standards Reporting Checklist . Information essential to interpreting the data presented should be made available in the figure legends.	
Have you included all the information requested in your manuscript?	
Resources	Yes
A description of all resources used, including antibodies, cell lines, animals and software tools, with enough information to allow them to be uniquely identified, should be included in the Methods section. Authors are strongly encouraged to cite Research Resource Identifiers (RRIDs) for antibodies, model organisms and tools, where possible.	

<p>Have you included the information requested as detailed in our Minimum Standards Reporting Checklist?</p>	
<p>Availability of data and materials</p> <p>All datasets and code on which the conclusions of the paper rely must be either included in your submission or deposited in publicly available repositories (where available and ethically appropriate), referencing such data using a unique identifier in the references and in the “Availability of Data and Materials” section of your manuscript.</p> <p>Have you have met the above requirement as detailed in our Minimum Standards Reporting Checklist?</p>	<p>Yes</p>

1 **Genome-scale metabolic modelling of responses to polymyxins in *Pseudomonas***
2 ***aeruginosa***

3 Yan Zhu¹, Tobias Czauderna², Jinxin Zhao¹, Matthias Klapperstueck², Mohd Hafidz

4 Mahamad Maifiah³, Mei-Ling Han³, Jing Lu⁴, Björn Sommer⁵, Tony Velkov⁶, Trevor

5 Lithgow¹, Jiangning Song¹, Falk Schreiber^{2,5*}, Jian Li^{1*,+}

6 ¹ Monash Biomedicine Discovery Institute, Department of Microbiology, Faculty of Medicine,
7 Nursing and Health Sciences, Monash University, Melbourne 3800, Australia; ² Faculty of
8 Information Technology, Monash University, Melbourne 3800, Australia; ³ Faculty of
9 Pharmacy and Pharmaceutical Sciences, Monash University, Melbourne 3052, Australia; ⁴
10 Monash Institute of Cognitive and Clinical Neurosciences, Department of Anatomy and
11 development biology, Faculty of Medicine, Nursing and Health Sciences, Monash University,
12 Melbourne 3800, Australia; ⁵ Department of Computer and Information Science, University of
13 Konstanz, Konstanz 78457, Germany; ⁶ Department of Pharmacology and Therapeutics,
14 University of Melbourne, Melbourne 3010, Australia.

15 **Email addresses:** YZ, yan.zhu@monash.edu; TC, tobias.czauderna@monash.edu; JZ,
16 jinxin.zhao@monash.edu; MK, matthias.klapperstueck@monash.edu; MHMM,
17 hafidz.maifiah@monash.edu; MLH, meiling.han@monash.edu; JLU, jing.lu2@monash.edu;
18 BS, bjoern.sommer@uni-konstanz.de; TV, tony.velkov@unimelb.edu.au; TL,
19 trevor.lithgow@monash.edu; JS, jiangning.song@monash.edu; FS, falk.schreiber@uni-
20 konstanz.de; JL, jian.li@monash.edu.

21 **Running title:** Metabolic modelling polymyxins responses

22 *Joint Senior authors. ⁺Corresponding author. 19 Innovation Walk, Monash University, VIC
23 3800, Australia. Tel: +61 3 9903 9702, Fax: +61 3 9902 9222, Email: jian.li@monash.edu.

24 Part of this work was presented at the 27th European Congress of Clinical Microbiology and
25 Infectious Diseases, 22-25 April 2017, Vienna, Austria.

26 **Abstract**

27 **Background:** *Pseudomonas aeruginosa* often causes multidrug-resistant infections in
28 immunocompromised patients and polymyxins are often used as the last-line therapy.
29 Alarming, resistance to polymyxins has been increasingly reported worldwide recently. To
30 rescue this last-resort class of antibiotics, it is necessary to systematically understand how *P.*
31 *aeruginosa* alters its metabolism in response to polymyxin treatment, thereby facilitating the
32 development of effective therapies. To this end, genome-scale metabolic model (GSMM) was
33 employed to analyse bacterial metabolic changes at the systems level.

34 **Findings:** A high-quality GSMM *iPAO1* was constructed for *P. aeruginosa* PAO1 for
35 antimicrobial pharmacological research. Model *iPAO1* encompasses an additional periplasmic
36 compartment and contains 3,022 metabolites, 4,265 reactions and 1,458 genes in total. Growth
37 prediction on 190 carbon and 95 nitrogen sources achieved an accuracy of 89.1%,
38 outperforming all reported *P. aeruginosa* models. Notably, prediction of the essential genes for
39 growth achieved a high accuracy of 87.9%. Metabolic simulation showed that lipid A
40 modifications associated with polymyxin resistance exert a limited impact on bacterial growth
41 and metabolism, but remarkably change the physiochemical properties of the outer membrane.
42 Modelling with transcriptomics constraints revealed a broad range of metabolic responses to
43 polymyxin treatment, including reduced biomass synthesis, upregulated amino acids
44 catabolism, induced flux through the tricarboxylic acid cycle, and increased redox turnover.

45 **Conclusions:** Overall, *iPAO1* represents the most comprehensive GSMM constructed to date
46 for a Gram-negative bacterium. It provides a powerful systems pharmacology platform for the
47 elucidation of complex killing mechanisms of antibiotics.

48 **Keywords:** Genome-scale metabolic model; *Pseudomonas aeruginosa*; polymyxin; lipid A
49 modification; outer membrane

50 Background

1
2
3 51 *Pseudomonas aeruginosa* is a common multidrug-resistant (MDR) pathogen in immune-
4
5 52 compromised patients, cystic fibrosis patients and burns victims [1-6]. It possesses a large
6
7 53 genome (5.5-7.0 Mb), complex regulatory networks, remarkable metabolic versatility and an
8
9 54 extraordinary ability to survive extremely harsh conditions such as prolonged antibiotic
10
11 55 exposure [7, 8]. Polymyxins (i.e. polymyxin B and colistin) have been increasingly used as a
12
13 56 last-line therapy to treat infections caused by MDR *P. aeruginosa* [9]. Alarminglly, the
14
15 57 prevalence of polymyxin resistance in *P. aeruginosa* has increased worldwide over the past
16
17 58 few years [3, 10, 11].
18
19
20
21

22
23 59 The exact mode of action of polymyxins is not clear except the initial electrostatic and
24
25 60 hydrophobic interactions with lipid A, a component of the lipopolysaccharide (LPS) in the
26
27 61 bacterial outer membrane (OM). Subsequently, cell envelope is disorganised, cellular contents
28
29 62 leak, oxidative stress increases, and finally cell death occurs [2, 9, 12, 13]. After polymyxin
30
31 63 treatment, *P. aeruginosa* modifies its lipid A structure to attenuate the aforementioned
32
33 64 electrostatic interactions [14]. Our recent metabolomics data demonstrated that, apart from
34
35 65 lipid A modifications, numerous biochemical pathways are perturbed by polymyxin treatment,
36
37 66 indicating that the development of polymyxin resistance by *P. aeruginosa* involves a
38
39 67 complicated interplay of multiple cellular processes [15]. There are significant gaps in the
40
41 68 knowledge-base of the mechanisms of polymyxin activity and bacterial responses in *P.*
42
43 69 *aeruginosa*, thereby necessitating comprehensive investigations using systems pharmacology
44
45 70 approaches.
46
47
48
49

50
51
52 71 With the rapid development of genome-scale metabolic models (GSMMs) and the associated
53
54 72 flux balance analysis (FBA) methods, systematic investigations into the metabolic changes in
55
56 73 response to external nutrient alterations, genetic perturbations, and antibiotic treatments are
57
58 74 now becoming feasible [16-24]. Four GSMMs have been constructed for *P. aeruginosa* and
59
60
61
62
63
64
65

1
2
3
4
5
6
7
8
9
10
11
12
13
14
15
16
17
18
19
20
21
22
23
24
25
26
27
28
29
30
31
32
33
34
35
36
37
38
39
40
41
42
43
44
45
46
47
48
49
50
51
52
53
54
55
56
57
58
59
60
61
62
63
64
65

75 they are iMO1056 [25], Opt208964 [26] , iMO1086 [27] and the latest iPae1146 [28]; among
76 which iMO1056 and Opt208964 share the same identifier systems and are fully accessible via
77 Model SEED [29]. The previous applications of these models have included simulating the
78 metabolic dynamics in cystic fibrosis patients [30], elucidating the mechanisms of biofilm
79 formation [31, 32], predicting potential drug targets [33-35] and identifying the key genes
80 controlling virulence factors [28]. As important as they have been, these models have several
81 overarching limitations. Those past models (i) do not include a major cellular component, the
82 periplasmic space; (ii) have poor representation of glycerophospholipid (GPL) biosynthesis;
83 and (iii) lack lipid A modification reactions. Considering the pathogenesis of *P. aeruginosa*,
84 these major limitations significantly compromise the modelling functions. In particularly, the
85 power of the four reported GSMMs to predict metabolic responses to antibiotic treatment is
86 very limited, as periplasmic GPL and LPS biogenesis play critical roles in responses to anti-
87 pseudomonal antibiotics such as polymyxins [15, 36-39].

88 Here we describe *iPAO1*, a newly developed GSMM for *P. aeruginosa* PAO1 based upon
89 Opt208964 [26] and iMO1056 [25] but with intensive manual curation using several major
90 databases and the literature. Most notably, *iPAO1* is the first GSMM for *P. aeruginosa* where
91 the periplasmic space compartment is incorporated to comprehensively represent cross-
92 membrane transport, GPL metabolism and LPS biosynthesis. To the best of our knowledge
93 *iPAO1* represents the most comprehensive metabolic reconstruction for *P. aeruginosa* PAO1
94 and the largest manually curated metabolic model for any Gram-negative bacterium thus far.
95 Modelling with *iPAO1* revealed that the lipid A modifications might exert limited impact on
96 cell growth and metabolism but change the physiochemical properties of bacterial OM.
97 Constrained by gene expression levels, the model was employed to elucidate the metabolic
98 responses to polymyxin B treatment. Together, *iPAO1* provides a powerful systems platform
99 for antimicrobial pharmacological research to combat the rapidly increasing resistance.

100

1
2
3
4
5
6
7
8
9
10
11
12
13
14
15
16
17
18
19
20
21
22
23
24
25
26
27
28
29
30
31
32
33
34
35
36
37
38
39
40
41
42
43
44
45
46
47
48
49
50
51
52
53
54
55
56
57
58
59
60
61
62
63
64
65

101 **Data Description**

102 The genome sequence and annotation of *P. aeruginosa* PAO1 were obtained from GenBank
103 (Accession NC_002516.2). Models iMO1056 and Opt208964 were retrieved from Model
104 SEED [29]. The gas chromatography–mass spectrometry (GC-MS) metabolomics data were
105 collected from the literature [40]. Metabolites, reactions and pathways were obtained from
106 biochemical databases KEGG (Kyoto Encyclopaedia of Genes and Genomes) [41], MetaCyc
107 [42], TCBD (Transporter Classification Database) [43], TransporterDB [44] and Pseudomonas
108 Genome DB [45]. Growth phenotypes on 190 carbon sources and 95 nitrogen sources were
109 determined using BIOLOG Phenotypic Microarrays. Non-essential gene lists were collected
110 from two previously reported transposon mutant libraries for PAO1 [46, 47]. Lipid A of wild-
111 type *P. aeruginosa* PAK and its polymyxin-resistant mutant PAK pmrB6 was extracted using
112 mild acid hydrolysis method and the structural analysis of lipid A was conducted using mass
113 spectrometry [39]. RNA was extracted and employed to construct cDNA libraries for RNA-
114 Seq on Illumina MiSeq platform [48]. The raw reads were quality trimmed and aligned to
115 PAO1 reference genome using SubRead [49]. Counts were normalised and the differential gene
116 expression was determined using voom/limma packages with Degust [50]. Whole-cell lipids
117 and intracellular metabolites were extracted using the single-phase Blich-Dyer method as
118 previously described and analysed by liquid chromatography-mass spectrometry (LC-MS) [14,
119 39]. Raw metabolomics data were processed with IDEOM software followed by bioinformatic
120 analysis [51].

121

122 **Analyses**

123 **Development of a superior GSMM for *P. aeruginosa* PAO1**

124 Initially, a draft model (*i*PAO1_draft1) containing 1,991 reactions, 1,579 metabolites and 1,021
125 genes was created based upon iMO1056 [25] and Opt208964 [26] (**Additional files 2-4**). To
126 obtain a high-quality GSMM, extensive manual curation was conducted. Firstly, *i*PAO1_draft1
127 was complemented using databases and the literature. Specifically, the following additional
128 information was incorporated into the draft model, 285 metabolites and 36 reactions from
129 KEGG [41], 225 metabolites and 50 reactions from MetaCyc [42], and 7 metabolites and 20
130 reactions obtained by previous GC-MS-based quantification [40] (**Additional files 5 and 6**).

131 Secondly, a periplasmic compartment was built to incorporate 698 periplasmic metabolites,
132 509 transport reactions across the inner membrane (IM), 441 transport reactions across the
133 outer membrane (OM), and 403 periplasmic reactions. The resulting intermediate model was
134 designated as *i*PAO1_draft2.

135 Thirdly, the major pathway gaps were filled. GapFind [52] identified 109 dead-end metabolites
136 (**Additional file 7**). The growth phenotypes on 190 carbon and 95 nitrogen nutrients were
137 predicted using *i*PAO1_draft2, and compared with our experimental BIOLOG Phenotypic
138 Microarray (PM) results (**Additional file 8**). As a result, 162 false negative predictions (i.e. the
139 prediction indicated non-growth whereas the BIOLOG experiment demonstrated valid growth
140 on a specific nutrient) were determined, indicating the lack of associated transport or catabolic
141 reactions for these nutrients. To link the dead-end metabolites back to the metabolic network
142 and eliminate inconsistencies with the BIOLOG PM results, several modifications were made
143 including (i) adjustment of the reversibility settings of 180 reactions and changing the
144 directions of 87 reactions (**Additional file 9**); (ii) removal of 14 metabolites and 96 reactions
145 (**Additional files 10 and 11**), which were either duplicated (e.g. β -D-glucose was duplicated
146 with D-glucose) or representing general metabolite classes (e.g. protein, mRNA, DNA); and
147 (iii) addition of 98 boundary reactions, 677 transport reactions, and 252 metabolic reactions
148 (**Additional file 12**). Resolving the false negative predictions of the BIOLOG growth

149 phenotypes substantially improved the model. For example, predictions using *iPAO1_draft2*
150 showed that PAO1 was unable to grow with formic acid as a sole carbon source due to the lack
151 of the corresponding transport reaction. Interrogating the Pseudomonas Genome Database [45]
152 and Pfam [53] identified PA2777, a hypothetical protein in NCBI and UniProt which may
153 encode formic/nitrite transporter (Pfam01226, $P=7e-34$). Subsequent addition of the transport
154 reaction (rxn08526) enabled *in silico* growth of PAO1 on formic acid. Another example is that
155 initially *iPAO1_draft2* failed to predict utilisation of 1,2-propanediol for growth owing to the
156 exiting gap in dehydrogenation of 1,2-propanediol to lactaldehyde. Using BLASTp with the
157 query sequence of lactaldehyde reductase (*fucO*, *b2799*) from *Escherichia coli* K12 MG1655
158 identified a candidate homologous gene PA1991 (Identity=35%, Eval=2e-75, BLASTp).
159 PA1991 encodes an iron-containing alcohol dehydrogenase and has over 300 orthologues in
160 Gram-negative bacteria which encode lactaldehyde oxidoreductases or 1,2-propanediol
161 dehydrogenases according to OrthoDB [54]. Inactivation of PA1991 resulted in 8-fold
162 prolonged lag phase when *P. aeruginosa* grew on 1,2-propanediol [55]. Therefore, reaction
163 rxn01615 oxidising 1,2-propanediol to lactaldehyde was added into *iPAO1_draft2*. A very
164 large number of such labour intensive manual curations were conducted to improve the model.
165 This enabled *in silico* growth on a number of nutrients from BIOLOG PM, including 4-
166 hydroxyphenylacetate, tyramine, quinic acid, itaconic acid, citramalic acid, L-pyroglutamic
167 acid, carnidine, glycinebetaine, L-methylsuccinate, and D-amino acids (**Additional file 8**).

168 Fourthly, the biogenesis of bacterial envelope was delineated. Cross-linking between amino
169 acids residues among peptidoglycan chains results in a rigid network structure in *P. aeruginosa*
170 [56]. In total, 17 reactions representing peptidoglycan cross-linking and hydrolysis were
171 incorporated by searching for homologues of glycosyltransferases, transpeptidases,
172 carboxypeptidases and endopeptidases in PAO1 [57]. Overall, a detailed peptidoglycan
173 biosynthesis pathway was constructed with 60 reactions. GPL compositions in the bacterial

174 membranes can change in response to antibiotic treatment [36, 58]. Previous studies [59] and
175 our own lipidomics results [14] showed a great diversity in GPL species in *P. aeruginosa*.
176 Overall, 386 unique metabolites (i.e. 66.2% of the 583 metabolites in the GPL metabolism
177 pathway) and 367 reactions (66.7% of the 550 reactions in the GPL metabolism pathway) were
178 incorporated into *iPAO1_draft2* (**Additional files 1, 13 and 14, Fig 1**). LPS consists of lipid
179 A, core oligosaccharide, and *O*-antigen polysaccharide [37], and plays key roles in the host-
180 pathogen interaction and the resistance to antibiotics such as polymyxins [13, 60]. A detailed
181 synthesis and interconversion network was generated with 432 types of LPS and 1,169
182 reactions (**Fig 2, Additional file 1**). Notably, our GSMM is the most comprehensive to date in
183 lipid A biosynthesis and modifications.

184 The resulting final *iPAO1* model consisted of 3,022 metabolites, 4,365 reactions and 1,458
185 genes (25.8% of the PAO1 genome, **Additional files 15-17**), representing, respectively, (i)
186 252%, 340% and 40% increase of the components in *iMO1056*; and (ii) 125%, 171% and 43%
187 increase of the components in *Opt208964* (**Table 1**). The significant expansion in *iPAO1*
188 includes cross-membrane transport, GPL/LPS biosynthesis, peptidoglycan biosynthesis, and
189 fatty acid degradation (**Additional files 15-17**). The reactions from *iPAO1* were categorised
190 into 109 pathways mainly based on classifications in MetaCyc and KEGG. In *iPAO1*,
191 27.9%/43.7%/51.6% metabolites, 20.3%/33.5%/59.5% reactions and 65.3%/17.6%/28.5%
192 genes are originated from *iMO1056*, *Opt208964*, and our manual curation, respectively (**Fig**
193 **3A**).

194 Components in *iPAO1* were aligned with databases including KEGG [41], MetaCyc [42],
195 PubChem [61], ChemSpider [62], ChEBI [63], Model SEED [29], and BiGG [64] (**Additional**
196 **files 15 and 16**). Consequently, 1,404 (46.5%), 1,590 (52.6%) and 2,142 (70.9%) metabolites
197 have corresponding identifiers in MetaCyc, KEGG and Model SEED, respectively; 1,556
198 (35.6%), 1,596 (36.6%) and 1,964 (45.0%) reactions were computationally mapped to the

199 reactions from MetaCyc, KEGG and Model SEED, accordingly (**Fig 3B**). A significant portion
200 of mismatches were caused by the incorporation of specific types of metabolites in the GPL
201 metabolism and LPS biosynthesis pathway, which in databases are usually lumped as general
202 compound classes. The properties of metabolites, including mass, charge and formula were
203 included in *iPAO1*. The standard Gibbs free energy change of formation ($\Delta_f G^\circ$), and reaction
204 ($\Delta_r G^\circ$) were obtained from MetaCyc and Model SEED for 1,877 metabolites (62.1%) and 1,355
205 reactions (31.0%) (**Additional files 15 and 16**).

206 A breakdown of genes involved in *iPAO1* (**Additional file 17**) using the clusters of orthologous
207 groups (COGs) showed remarkable improvement compared to previous reconstructions (**Fig**
208 **3C**). The largest increase in the coverage compared to *iMO1056* is lipid transport and
209 metabolism (24.1%), followed by inorganic ion transport and metabolism (19.3%); whereas
210 compared to *Opt208964*, the largest increase in the coverage is nucleotide transport and
211 metabolism (57.9%), followed by amino acid transport and metabolism (52.0%). Overall, the
212 transport and metabolism of nucleotides and amino acids showed the highest percent coverage
213 of COG functional categories in *iPAO1* (72.9% and 65.6%, respectively). Notably, the
214 reactions in categories not apparently related to metabolism were dramatically reduced in
215 *iPAO1* compared to *Opt208964*, including translation, ribosomal structure and biogenesis,
216 posttranslational modification, protein turnover, chaperones and signal transduction
217 mechanisms, or undetermined categories including function unknown class. Therefore, *iPAO1*
218 is a well-defined, metabolism-dedicated model.

219 In the new *iPAO1* model, the pathways GPL metabolism, LPS biosynthesis and transport
220 across OM were ranked the three largest pathways and also contained the highest proportion
221 of curated reactions (**Fig 3D**). Additionally, these three pathways have high reaction-to-gene
222 ratios (13.1-24.2, **Fig 3E**), indicating that enzymes in these pathways are capable of acting on
223 a broad range of substrates. As kinetic parameters are usually not involved in a GSMM,

224 constraint-based analyses (e.g. FBA) of a GSMM do not directly account for enzyme levels,
225 intracellular metabolic concentrations or substrate-level regulation. Accordingly, the affinity
226 difference of various substrates was not considered in our *iPAO1* modelling effort.

227 We employed the biomass formation equation from iMO1056 to construct *iPAO1* with
228 modifications on LPS and ion species (**Additional file 18**). In addition, to take into account the
229 extra energy consumption caused by charging tRNAs, the original amino acids in the biomass
230 formation reaction were replaced by aminoacyl-tRNA, followed by addition of specific
231 charging reactions to the model. Taken together, *iPAO1* represents the most comprehensive
232 metabolic reconstruction thus far for *P. aeruginosa* PAO1.

233 **Growth capability on various nutrients**

234 Investigation of nutrient utilisation using BIOLOG PM showed PAO1 could utilise a broad
235 range of nutrient sources, indicated by the observed growth on 68 of 190 (35.8%) carbon and
236 76 of 95 (80.0%) nitrogen substrates (**Fig 4**). Growth simulation with *iPAO1* achieved an
237 overall accuracy of 89.1% (254 of 285), which substantially outperformed previous models
238 (81.5% for Opt208964 [26], 77.9% for iMO1056 and iMO1086 [27] and 80% for iPae1146
239 [28]. Twenty-one false-positive and 10 false-negative (**Fig 4, Additional file 8**) disagreements
240 were observed, possibly due to the complexity of regulatory mechanisms and missing
241 annotation of nutrient transport and/or catabolism pathways in PAO1.

242 **Prediction and validation of gene essentiality**

243 *In silico* single-gene deletion with *iPAO1* showed 143 essential genes ($\mu_{mut} < 0.01 \mu_{wt}$), 40 semi-
244 essential genes ($0.01 \mu_{wt} < \mu_{mut} < 0.99 \mu_{wt}$), and 1,275 non-essential genes ($0.99 \mu_{wt} < \mu_{mut} < \mu_{wt}$)
245 when growing in Luria-Bertani (LB) media (**Additional file 19**). Among the essential
246 metabolic genes, the largest COG proportion (46 of 143, 32.1%) is cell envelope biogenesis,
247 indicating that there are relatively less alternative reactions in this pathway. For non-essential

248 genes, amino acid transport and metabolism (352 of 1,315, 26.7%) represents the largest group,
249 suggesting the existence of large metabolic redundancy.

250 The predicted gene essentiality was further verified by two independent genome-scale
251 transposon mutant libraries [46, 47, 65]. The overall prediction accuracy achieved 87.9%,
252 which is higher than iMO1056 (85.0%) [25] and iMO1086 (84.2%) [27], but slightly lower
253 than Opt208964 (92.9%) [26] and iPae1146 (91.46%) [28]; this is possibly due to the
254 incorporation of new genes (30.5% increase compared to Opt208964; 27.2% increase
255 compared to iPae1146) whose metabolic functions were previously misannotated.

256 **Impact of lipid A modifications on bacterial growth and metabolism**

257 *P. aeruginosa* modifies lipid A components in the OM in response to polymyxin treatment [66].
258 The LPS stoichiometric coefficients in the biomass formula of *iPAO1* were configured based
259 on our lipidomics data (**Table 2**, [14]), to predict the metabolic impact of lipid A modifications
260 (see Methods Section for details). Overall, 273 fluxes were significantly affected (Z-Score,
261 false discovery rate (FDR) <0.01 ; >0.1 mmol·gDW·h⁻¹ under at least one condition, **Additional**
262 **file 20**). The specific growth rate remained unchanged. A 0.026 mmol·gDW·h⁻¹ flux from
263 glucose via glucose 6-phosphate, uridine diphosphate glucose, and consequently 4-amino-4-
264 deoxy-L-arabinose (L-Ara4N) biosynthesis was identified due to lipid A modifications. The
265 overall fluxes through lipid A deacylation reactions were increased (from 0.007 mmol·gDW·h⁻¹
266 ¹ to 0.011 mmol·gDW·h⁻¹); the generated (*R*)-3-hydroxydecanoate was fuelled into β -oxidation
267 to produce octanoyl-CoA, which was subsequently salvaged for fatty acid biosynthesis.

268 To further investigate the impact of lipid A modifications on bacterial growth, 1,000 sets of the
269 compositions of 288 heterogeneous LPS molecules were randomly generated with the total
270 proportion of LPS unchanged in the biomass formation formula (**Additional file 21**). The
271 metabolic fluxes were calculated for each of the 1,000 sets of LPS compositions using FBA.

272 Across the 1,000 sets of metabolic fluxes (**Additional file 23**), the specific growth rate varied
273 between 0.8812 and 0.8897 mmol·gDW·h⁻¹. Correlative analysis of the apparent overall
274 physiochemical properties of lipid A (**Additional file 22**) with the predicted growth phenotypes
275 showed three interesting findings. Firstly, addition of L-Ara4N reduced the negative charge of
276 lipid A ($\rho=1.00$), decreased the hydrophobicity of the OM (represented by logP, $\rho=-0.59$), but
277 required assimilation of more ammonia (represented by ammonia turnover, $\rho=0.57$). Secondly,
278 hydroxylation on acyl chains of lipid A exerted minor effects over either bacterial growth or
279 physiochemical properties. Thirdly, addition of acyl chains resulted in large lipid A molecules
280 (represented by the atomic counts, $\rho=0.88$), enhanced molecular polarity of lipid A ($\rho=0.87$),
281 increased OM hydrophobicity ($\rho=0.75$), and notably, retarded growth ($\rho=-0.95$), reduced redox
282 and energy turnover ($\rho=-0.98$ for both), and increased requirement of ammonia ($\rho=0.59$) (**Fig**
283 **5**). It is evident that none of the three aforementioned modifications produced a dramatic impact
284 on bacterial growth or metabolism (**Additional file 23**).

285 **Elucidating the mechanisms of metabolic responses to polymyxin treatment**

286 RNA-Seq data were utilised as model constraints (**Additional file 24**) to calculate the
287 metabolic fluxes in the absence and presence of polymyxin B (*cf.* Methods). Comparison of
288 the flux distributions revealed that 1,392 reactions were differentially regulated (FDR<0.01,
289 **Additional file 25**). A range of metabolic pathways were significantly disturbed, including
290 central metabolism, amino acid metabolism, purine biosynthesis, fatty acid biosynthesis and
291 metabolism, LPS and GPL biosynthesis and transport reactions. Polymyxin B treatment
292 reduced the growth rate (18.2%), increased oxygen uptake (6.9%) and CO₂ emission (6.0%);
293 however, the respiration quotient remained roughly unchanged (**Table 3**).

294 As the major carbon sources, the amino acids and oligopeptides from cation-adjusted Mueller-
295 Hinton broth (CAMHB) were utilised to generate intermediate metabolites, redox and energy

296 equivalents for biomass formation. In response to polymyxin treatment, the gluconeogenesis
297 pathway was significantly induced from pyruvate to 3-phosphoglycerate, but suppressed from
298 3-phosphoglycerate towards glucose 6-phosphate. The extra flux from 3-phosphoglycerate was
299 shunt to serine and glycine biosynthesis (**Fig 6**) via 3-phospho-D-glycerate:NAD⁺
300 oxidoreductase (rxn01101), 3-phosphoserine:2-oxoglutarate aminotransferase (rxn02914), *O*-
301 phospho-L-serine phosphohydrolase (rxn00420), and 5,10-methylenetetrahydrofolate:glycine
302 hydroxymethyltransferase (rxn00692), through which more NADH equivalent was generated
303 compared to the control. The resulting one-carbon unit in 5,10-methylenetetrahydrofolate was
304 oxidised to formic acid via 10-formyltetrahydrofolate amidohydrolase (rxn00691); the
305 generated glycine was fuelled into TCA cycle via glycine:oxygen oxidoreductase (rxn00269)
306 and acetyl-CoA:glyoxylate C-acetyltransferase (rxn00330). In addition, the metabolic flux via
307 TCA cycle was upregulated from citrate to fumarate, with increased NADH production. Within
308 oxidative phosphorylation, the mean fluxes through NADH dehydrogenase (Complex I,
309 rxn10122), cytochrome bc1 complex (Complex III, rxn13820), and cytochrome c oxidase
310 (Complex IV, rxn13688) decreased by 6.6%, 7.2% and 7.8%, respectively. The flux via F₀F₁-
311 ATPase (Complex V, rxn10042) was downregulated by 11.1%. The overall fluxes via
312 biosynthesis of macromolecules including LPS, GPL and peptidoglycan decreased due to the
313 significantly reduced biomass formation. The biosynthesis of spermidine increased by 38.3%
314 in response to polymyxin treatment which was also indicated by upregulated expression of
315 *speD* (PA4773; encoding the *S*-adenosyl-L-methionine decarboxylase, log₂FC=3.62,
316 FDR<0.01) and *speE* (PA4774; encoding spermidine synthase, log₂FC = 3.54, FDR<0.01).

317 Calculating the flux-sum of critical cofactors revealed 13.1% increase of redox turnover and
318 8.2% decline of energy turnover after 1 mg/L polymyxin B treatment for 1 h. Breaking down
319 the cofactors showed the turnover of major redox equivalents NADH, NADPH, ubiquinol-8
320 and FADH₂ substantially increased by 12.6%, 13.9%, 3.9% and 35.9%, respectively; whereas

1 321 the turnover of ATP, the major contributor to energy significantly decreased by 8.52% after 1
2 322 mg/L polymyxin treatment for 1 h (**Fig 6, Additional file 26**). Overall, metabolic flux analysis
3
4 323 using *iPAO1* integrated with our transcriptomics data revealed a significant global impact on
5
6
7 324 bacterial metabolism due to polymyxin B treatment.
8
9

10 325

11 12 13 326 **Discussion**

14
15
16 327 The emergence of Gram-negative ‘superbugs’ that are resistant to the last-resort polymyxins
17
18 328 highlights the urgent need for novel approaches such as GSMMs to understand the mechanisms
19
20
21 329 of antibacterial activity and resistance. The main utility of GSMMs is their ability to bridge
22
23 330 critical gaps between genomics and metabolic phenotypes through the prediction of metabolic
24
25
26 331 responses to antimicrobial treatments at the network level. Here, we report the development,
27
28 332 optimisation, validation and application of a high-quality GSMM designated *iPAO1* for a type
29
30
31 333 strain *P. aeruginosa* PAO1; and importantly, *iPAO1* was employed to understand the
32
33 334 complicated effect of polymyxin treatment on bacterial metabolism. Simulation with *iPAO1*
34
35
36 335 showed that lipid A modifications in response to polymyxin treatment only exert minor effects
37
38 336 on bacterial growth and metabolism. Albeit, further calculations that integrate transcriptomics
39
40
41 337 data as model constraints revealed that polymyxin treatment may reduce growth and affect a
42
43 338 broad range of pathways.

44
45
46 339 *iPAO1* represents the most comprehensive metabolic model for *P. aeruginosa* to date and
47
48 340 incorporates 1,458 genes, accounting for ~25.8% of the PAO1 genome. Among the four
49
50
51 341 GSMMs developed for *P. aeruginosa* PAO1, *iMO1086* and *iPae1146* were constructed on the
52
53 342 basis of *iMO1056* with moderate increase of metabolites, reactions and genes [25, 27, 28];
54
55
56 343 *Opt208964* is also in a medium size, which limits modelling capacity [26]. In contrast, *iPAO1*
57
58 344 is significantly expanded in model scale, by doubling or even tripling the numbers of
59
60
61
62
63
64
65

1
2
3
4
5
6
7
8
9
10
11
12
13
14
15
16
17
18
19
20
21
22
23
24
25
26
27
28
29
30
31
32
33
34
35
36
37
38
39
40
41
42
43
44
45
46
47
48
49
50
51
52
53
54
55
56
57
58
59
60
61
62
63
64
65

345 metabolites and reactions (**Fig 3A**). *iPAO1* achieved an unprecedented prediction accuracy of
346 89.1% for growth on various nutrients, outperforming all of the previously reported GSMMs
347 for *P. aeruginosa* [25-28]. The *iPAO1* model was also employed to predict gene essentiality
348 with a high accuracy of 87.9%. Given the extensive curation and significant expansion, *iPAO1*
349 will serve as the primary reference for future development of metabolic models, particularly
350 for other *P. aeruginosa* strains.

351 Unlike *iPAO1*, none of the previous *P. aeruginosa* GSMMs incorporated the periplasm. As
352 polymyxins initially target LPS in the OM and can cause substantial changes in the cell
353 envelope, the periplasmic space is a major component in *iPAO1*. The periplasmic space of *E.*
354 *coli* is estimated to constitute up to 16% of total cell volume [67]. It contains a thin cell wall
355 composed of peptidoglycan and a variety of ions and proteins, which are involved in transport,
356 folding, cell envelope biogenesis, electron transport and xenobiotic metabolism [68]. *iPAO1* is
357 the first *P. aeruginosa* GSMM to incorporate the periplasmic compartment, enabling accurate
358 representation of metabolic machinery, especially for those reactions that occur exclusively in
359 this important cellular space and transport of substrates across the IM and OM. Furthermore,
360 *iPAO1* provides detailed representations of GPL and LPS biosynthesis which allows the
361 precise mapping of GPL and LPS responses from experimental metabolomics and lipidomics
362 data (**Figs 1 and 2**).

363 In response to polymyxin treatment, Gram-negative bacteria modify their lipid A with cationic
364 moieties (i.e. phosphoethanolamine and L-Ara4N) that act to repel the like-charge of the
365 polymyxin molecule [37]. Based on our simulations (**Additional file 20**), we purport that such
366 lipid A modifications exerted a limited impact on cellular metabolism and growth. Most of the
367 flux changes were insignificant; the remaining significant flux changes mainly resulted from
368 futile cycles containing sets of reactions using redox equivalents, whereas the net carbon flow
369 remained unchanged. Simulation using randomised lipid A compositions further consolidated

1
2
3
4
5
6
7
8
9
10
11
12
13
14
15
16
17
18
19
20
21
22
23
24
25
26
27
28
29
30
31
32
33
34
35
36
37
38
39
40
41
42
43
44
45
46
47
48
49
50
51
52
53
54
55
56
57
58
59
60
61
62
63
64
65

370 our hypothesis that lipid A modifications cause only moderate variations of bacterial growth
371 and metabolism (**Fig 5, Additional file 23**). Notwithstanding, our simulation results revealed
372 that lipid A modifications result in substantial physiochemical changes in the OM of *P.*
373 *aeruginosa*, including (i) neutralising the surface negative charge by addition of positively
374 changed L-Ara4N; and (ii) altering the polarity and hydrophobicity by acylation and
375 deacylation. The general mode of action of polymyxin involves the initial electrostatic
376 interaction between the cationic side chains of the polymyxin molecule with the anionic lipid
377 A head groups [60]. These events are subsequently followed by hydrophobic interactions
378 between the *N*-terminal fatty acyl chain and position 6/7 hydrophobic side chains of the
379 polymyxin with the hydrophobic fatty acyls of lipid A [60]. Therefore, in concept both the
380 addition of L-Ara4N and deacylation of lipid A should contribute to polymyxin resistance.
381 Indeed, our recent transcriptomic and neutron reflectometry studies discovered that deletion of
382 the corresponding gene *pagL* (PA4661) resulted in an increased susceptibility to polymyxins,
383 in a polymyxin-resistant mutant PAK*pmrB6* derived from *P. aeruginosa* PAK [14, 69],
384 demonstrating that the lipid A deacylation also plays a key role in the response of *P. aeruginosa*
385 to polymyxin treatment.

386 Our recent transcriptomics and metabolomics studies discovered that polymyxin treatment
387 leads to remarkable growth reduction and metabolic perturbations in Gram-negative bacteria
388 [38, 39, 70-72]. The integration of transcriptomics results into GSMMs allow for more accurate
389 predictions of metabolic responses to either environmental (i.e. antibiotic treatment) or genetic
390 perturbations (i.e. mutations) [73]. In the present study, we employed the E-Flux method to
391 integrate transcriptomics data as flux constraints [74]. E-Flux can map continuous gene
392 expression levels to the metabolic network and uses the transcript abundance to determine the
393 degree to which a reaction is active or inactive [74]. Therefore, E-Flux provides a more
394 physiologically relevant description of the continuous nature of the reaction activity and avoids

1
2
3
4
5
6
7
8
9
10
11
12
13
14
15
16
17
18
19
20
21
22
23
24
25
26
27
28
29
30
31
32
33
34
35
36
37
38
39
40
41
42
43
44
45
46
47
48
49
50
51
52
53
54
55
56
57
58
59
60
61
62
63
64
65

395 to use any artificial thresholds to binarise gene expression data [75]. Comparison of the
396 calculated flux distributions revealed that a broad range of metabolic perturbations occur in
397 response to polymyxin treatment (**Fig 6**), ranging from central carbon metabolism to oxidative
398 phosphorylation and amino acid metabolism. Reduced growth, increased redox turnover and
399 decreased energy turnover due to polymyxin treatment were evident (**Fig 6**), indicating that
400 bacterial cells regulated their metabolism to produce more redox power to cope with the
401 oxidative stress. This is consistent with previous findings that showed bactericidal antibiotics
402 induced lethal oxidative damages via generating highly deleterious free radicals with
403 subsequent culmination of cellular death [76]. In addition, our simulations revealed that
404 polymyxin treatment induced an uptake of L-alanine, which was catabolised to generate more
405 NADH (**Fig 7**). This indicates that rich media (e.g. CAMHB) may provide abundant amino
406 acids and peptides that can be utilised by bacterial cells to generate sufficient redox equivalents
407 to cope with the oxidative damage caused by polymyxin treatment. Furthermore, our
408 simulation results also showed an upregulated metabolic flux towards L-spermidine
409 biosynthesis upon polymyxin B treatment (rxn00127 and rxn01406, **Additional file 25**).
410 Previous studies showed that polyamines (e.g. spermidine) could protect *P. aeruginosa* from
411 antimicrobial peptide killing [77]. It is assumed that the cationic spermidine could interact with
412 the anionic LPS, mask the negative cell surface, and reduce the electrostatic interactions
413 between polymyxin B and bacterial OM. Therefore, the enhanced biosynthesis of spermidine
414 might increase its abundance at the cell surface and contribute to polymyxin resistance.

415 The constructed *i*PAO1 provides a detailed presentation of LPS biogenesis (**Fig 2**), in particular
416 lipid A modifications. Further integration with specific regulatory modules will enable
417 dynamic simulation of metabolic responses to polymyxin treatment. Previous studies revealed
418 that various two-component regulatory systems (2CSs), including PhoPQ, PmrAB, ParRS,
419 CprRS and ColRS, play key roles in regulating polymyxin resistance [78-82]. Among them,

1
2
3
4
5
6
7
8
9
10
11
12
13
14
15
16
17
18
19
20
21
22
23
24
25
26
27
28
29
30
31
32
33
34
35
36
37
38
39
40
41
42
43
44
45
46
47
48
49
50
51
52
53
54
55
56
57
58
59
60
61
62
63
64
65

420 the PmrAB and PhoPQ systems are able to sense the depletion of external cations (e.g. Mg²⁺
421 and Ca²⁺) and upregulate the expression of the *arnBCADTEF-ugd* operon which is responsible
422 for the modification of lipid A with L-Ara4N [83]. Moreover, the fatty acylation of lipid A by
423 PagP is under the control of PhoPQ [84, 85]. ParRS and CprRS are independent 2CSs that
424 mediate the upregulation of *pmrAB*, *arnBCADTEF-ugd* operon, *pagL* and adaptive resistance
425 in response to polymyxin treatment [78, 86]. In overview, lipid A modifications due to
426 polymyxin treatment are strictly controlled by very complex regulatory networks involving
427 signal sensors, transcriptional regulators, and metabolic enzymes. Therefore, future studies are
428 warranted to integrate these regulatory modules into the GSMM to enable simulating bacterial
429 response dynamics to polymyxin treatment and analysing adaptive resistance mechanisms in
430 *P. aeruginosa*.

431 Overall, we have constructed, optimised and validated a high-quality genome-scale metabolic
432 model *iPAO1* for *P. aeruginosa* PAO1. This comprehensive model incorporates metabolic
433 pathways, particularly the biogenesis of membrane components, and enables delineating the
434 complex metabolic responses to antibiotics. *iPAO1* provides a valuable systems tool for
435 quantitative simulation of bacterial metabolic responses to antibiotics, elucidation of the
436 molecular mechanisms of antimicrobial killing and resistance, and facilitation of designing
437 rational antimicrobial combination therapy. To the best of our knowledge, this study is the first
438 to integrate antimicrobial pharmacology, computational biology, metabolic network and
439 systems pharmacology to analyse large-scale datasets, in order to better understand the
440 dynamic and complex nature of polymyxin killing and resistance. Combined with antibiotic
441 pharmacokinetics and pharmacodynamics, *iPAO1* offers an *in silico* platform for precision
442 antimicrobial pharmacology therapy.

443
444 **Potential implications**

1 445 The generated collection of transcriptomics metabolomics, lipidomics and lipid A profiling
2 446 data provides comprehensive datasets of *P. aeruginosa* for future integrative analysis of
3
4 447 polymyxin systems pharmacology. As the largest curated GSMM thus far for any Gram-
5
6
7 448 negative bacteria, *i*PAO1 represents all aspects of the cellular metabolism and may serve as the
8
9 449 platform for integrative analysis of multi-omics data. Simulation with transcriptomics
10
11 450 constraints in this study revealed metabolic flux changes in amino acid catabolism,
12
13 451 tricarboxylic acid cycle, and redox turnover caused by polymyxin treatment. Correlative
14
15 452 analysis of metabolomics and transcriptomics with the constraint-based modelling is necessary
16
17 453 for delineating the regulatory effects on metabolism. The methodology of using GSMMs to
18
19 454 analyse multi-level omics data is applicable to other areas beyond antimicrobial pharmacology.
20
21
22 455 Further integration with antimicrobial pharmacokinetics and pharmacodynamics will not only
23
24 456 provide better pharmacological understanding, but also empower the model to quantitatively
25
26 457 predict the bacterial responses to antimicrobial therapy in the context of complex interplay of
27
28 458 signalling, transcriptional regulation and metabolism. In summary, our GSMM approach
29
30 459 provides a powerful systems tool to elucidate the complex mode of action of antibiotics and
31
32 460 will paradigm shift antimicrobial pharmacology.
33
34
35
36
37
38
39
40
41

40 461

42 462 **Methods**

45 463 **Strain, media and BIOLOG experiments**

47
48 464 *P. aeruginosa* PAO1 was cultured in Luria-Bertani (LB) media and subcultured on nutrient
49
50 465 agar. Cells were swapped into sterile capped tube containing 16 mL IF-0 solution (Cell
51
52 466 Biosciences, West Heidelberg, Australia) till the turbidity achieved 42% transmittance in a
53
54 467 Turbidimeter (Pacificlub, Blackburn, Australia). The cell suspension was then diluted 5 times
55
56 468 with IF-0 solution and dye (Cell Biosciences) to final 85% transmittance. BIOLOG PM 1-3
57
58
59
60
61
62
63
64
65

1
2
3
4
5
6
7
8
9
10
11
12
13
14
15
16
17
18
19
20
21
22
23
24
25
26
27
28
29
30
31
32
33
34
35
36
37
38
39
40
41
42
43
44
45
46
47
48
49
50
51
52
53
54
55
56
57
58
59
60
61
62
63
64
65

469 (Cell Biosciences, Heidelberg, Australia) were used to investigate the carbon and nitrogen
470 utilisation with two independent biological replicates. Sodium succinate was used as the carbon
471 source for examining nitrogen utilization. Growth was detected after 24-h incubation at 37°C,
472 using an Infinite M200 microplate reader (Tecan, Mannedorf, Switzerland) at 595 nm.
473 Readings that were ≥ 1.5 -fold of the negative control (i.e. growth media without bacteria)
474 indicated the utilisation of nutrients.

475 **Development of a GSMM for *P. aeruginosa* PAO1**

476 To expedite the model development, two curated models for PAO1 with the same identifier
477 systems from Model SEED [29], iMO1056 [25] and Opt20896434 [26] were merged.
478 Databases including KEGG [41], MetaCyc [42], Pseudomonas Genome DB [45] and the
479 literature were employed to complete the model with missing components. The identifiers of
480 metabolites and reactions were kept consistent with Model SEED [26], and cross-referred to
481 MetaCyc, KEGG, PubChem [61], ChEBI [63], ChemSpider [62] and BiGG [64]. The PAO1
482 genome annotation from Pseudomonas Genome DB [45] was employed to construct ‘gene to
483 protein to reaction’ (GPR) associations [87]. A periplasm compartment was incorporated into
484 the model. Reactions and metabolites were then assigned to cytoplasm, periplasm and external
485 environment according to the localisation prediction of metabolic enzymes by PSORTb 3.0
486 [88]. Transport reactions were generated to enable material exchange across membranes
487 according to TCBD [43] and TransporterDB [44]. The model was constructed using the
488 Systems Biology Markup Language (SBML) [89, 90]. VANTED [91] was employed for
489 visualisation and analysis of the metabolic network. For each metabolite in the model, specific
490 features including compartment localisation, mass, charge, formula, formation free energy,
491 database identifiers and source were added (**Additional file 14**). Each reaction entered into the
492 model was checked with elementary and charge balance. Reversibility was determined first
493 from the primary literature for each particular enzyme or reaction, if available. Further curation

1
2 494 on reaction reversibility and directions was conducted based on change of free energy and
3 495 knowledge about the physiological direction of a reaction in a pathway.
4

5 496 The Gapfind function from the COBRA toolbox [92] was employed to identify the isolated and
6
7 497 dead-end metabolites in the model. Candidate reactions from KEGG, MetaCyc and BiGG were
8
9
10 498 manually inspected for relevance and homology evidence using BLASTp; reactions catalysed
11
12 499 by homologous enzymes (E-value<1×10⁻⁵, identity≥35%, coverage≥50%) were added to the
13
14
15 500 model to eliminate the gaps. Mispredictions of BIOLOG growth phenotypes were employed to
16
17 501 refine the draft model (*i*PAO1_draft2). Further curation was performed to represent the
18
19
20 502 complex biosynthesis pathways of macromolecules (e.g. peptidoglycan, GPL and LPS).
21

22
23 503 The biomass formation equation consisting of necessary building blocks for bacterial growth
24
25 504 was created using the one from iMO1086 [27], with slight modifications on compositions of
26
27
28 505 ions, peptidoglycans, GPL and LPS (**Additional file 17**). The growth and non-growth
29
30 506 associated maintenance was from iMO1086 [27].
31

32 33 507 **Growth prediction in BIOLOG media**

34
35
36 508 *i*PAO1 was employed to predict the growth phenotypes on chemically-defined media with 190
37
38
39 509 carbon and 95 nitrogen sources (**Additional file 18**) using the FBA method [24]. The objective
40
41 510 function of biomass formation was maximised with the specific nutrient uptake rate set at 10
42
43 511 mmol·gDW·h⁻¹ under aerobic condition.
44

45
46 512
$$\max \quad v_{\text{biomass}}$$

47
48
49 513
$$s. t. \quad \mathbf{Sv} = 0$$

50
51
52 514
$$a_i \leq v_i \leq b_i, i = 1, 2, \dots, n$$

53
54
55 515 where v_{biomass} denotes the biomass formation flux, \mathbf{S} represents the stoichiometric matrix and
56
57
58 516 each metabolic flux v_i was constrained by lower and upper bound a_i and b_i , respectively. All
59
60
61
62
63
64
65

1 517 modelling procedures were performed with the COBRA toolbox [92] in MATLAB. The
2 518 calculated specific growth rates ν_{biomass} were then compared to the BIOLOG PM data to assess
3
4 519 the prediction accuracy using Fisher's exact test.
5
6

7 520 **Gene essentiality prediction**

8
9
10 521 *In silico* single-gene deletion was performed using the CORBRA toolbox and the mutant
11
12 522 models were then used to predict the specific growth rate in LB broth [29] using FBA. Genes
13
14 523 with 99% reduction of the specific growth rate relative to the wild type were defined as essential
15
16 524 for cell growth; otherwise, they were considered as semi-essential (1-99% reduction) and non-
17
18 525 essential (<1% reduction). Two existing PAO1 transposon insertion mutant libraries, (i) two-
19
20 526 allele mutant library [47, 65] and (ii) mini-Tn5 insertion mutant library [46], were employed
21
22
23 527 to assess the overall prediction accuracy with Fisher's exact test.
24
25
26
27

28 528 **Simulation of bacterial growth and metabolic phenotype changes in response to lipid A** 29 30 529 **modifications**

31
32
33 530 The LPS stoichiometric coefficients in the biomass formula under the control and lipid A
34
35 531 modification conditions were set according to the measured lipid A compositions in the wild-
36
37 532 type *P. aeruginosa* PAK and its polymyxin-resistant mutant PAK $_{pmrB6}$, respectively (**Table**
38
39 533 **2**) [14]. For PAK $_{pmrB6}$, a missense mutation (L243Q) in *pmrB* resulted in constitutive
40
41 534 activation of the PmrAB system and induced expression of the regulated genes regardless of
42
43 535 polymyxin, including *arn* operon and *pagL* [39, 93]. Aerobic growth was simulated on minimal
44
45 536 media with glucose uptake at $10 \text{ mmol} \cdot \text{gDW}^{-1} \cdot \text{L}^{-1}$. For each simulation, the solution space was
46
47 537 sampled with 10,000 random points using the ll-ACHRB algorithm [94]. Flux samples of the
48
49 538 control and lipid A modification were then compared. Significantly perturbed metabolic fluxes
50
51 539 were identified using a Z-score based approach [95].
52
53
54
55
56
57

58 540 To further analyse the metabolic impact of lipid A modifications, the proportions of all types
59
60
61
62
63
64
65

1
2
3
4
5
6
7
8
9
10
11
12
13
14
15
16
17
18
19
20
21
22
23
24
25
26
27
28
29
30
31
32
33
34
35
36
37
38
39
40
41
42
43
44
45
46
47
48
49
50
51
52
53
54
55
56
57
58
59
60
61
62
63
64
65

541 of LPS in the biomass formula were randomly assigned and the process was repeated 1,000
542 times. For each repetition, the specific growth rates were calculated and solution space was
543 sampled using the methods above. For each type of lipid A, specific physiochemical properties
544 (*f*) including total atom number, partition coefficient (logP), average charge and molecular
545 polarity were predicted at pH 7 using the cxcalc tool from ChemAxon (Budapest, Hungary).
546 The overall apparent properties *F* of the OM were estimated by calculating the weighted sum.

$$F = \sum_{i=1}^n w_i f_i$$

547
548 where w_i represents the stoichiometric coefficient of the *i*-th of 288 heterogeneous LPS
549 molecules in the biomass formula. Pairwise correlation analysis was conducted between lipid
550 A modifications, physiochemical properties changes, bacterial growth and metabolism
551 alterations.

552 **Predict metabolic responses to polymyxin treatment by constraining fluxes with** 553 **transcriptomics data**

554 The RNA-Seq data from 1-h 1 mg·L⁻¹ polymyxin B treatment experiment using PAO1 were
555 employed as flux constraints for modelling [48]. For each gene under every condition, the
556 RPKM (Reads Per Kilobase Million) value was calculated from the aligned reads using the
557 edgeR package [96], and normalised to constrain flux upper bounds using the E-Flux algorithm
558 [74]. Since CAMHB was used in the RNA-Seq experiment, the maximum uptake rates of
559 amino acids, vitamins and dipeptides in *i*PAO1 were set to 1 mmol·gDW·h⁻¹ considering that
560 these nutrients in CAMHB provided the major carbon sources for bacterial growth. For each
561 condition, the solution space was sampled with 10,000 points using ll-ACHRB as above.
562 Statistical significance of differential flux distributions was computed using the Z-score method
563 above. The turnover rate for key metabolites was calculated by summing up all influxes or

1
2
3 564 effluxes [97].
4

5
6 565

7
8
9 **566 Availability of supporting data and materials**

10
11 567 The raw RNA-Seq data have been deposited in the NCBI Sequence Read Archive (SRA)

12 database under the BioProject accession number (to be updated). The metabolomics and

13 569 lipidomics data have been deposited in Metabolight database with the accession number (to be

14 updated).
15
16 570

17
18
19 571

20
21
22 **572 Additional files**

23
24
25 573 Additional file 1 (additionalFile1.docx): Manual curation of GPL biosynthesis, LPS

26 biosynthesis and modification pathways.
27
28 574

29
30 575 Additional file 2 (additionalFile2.xlsx): Metabolites in the constructed draft model

31 *i*PAO1_draft1.
32
33 576

34
35
36 577 Additional file 3 (additionalFile3.xlsx): Reactions in the constructed draft model *i*PAO1_draft1.

37
38
39 578 Additional file 4 (additionalFile4.xlsx): Genes in the constructed draft model *i*PAO1_draft1.

40
41
42 579 Additional file 5 (additionalFile5.xlsx). Supplemented metabolites according to previous GC-

43 MS based metabolomics data.
44
45 580

46
47 581 Additional file 6 (additionalFile6.xlsx): Supplemented reactions according to previous GS-MS

48 based metabolomics data.
49
50 582

51
52 583 Additional file 7 (additionalFile7.xlsx): Root gap metabolites identified using GapFind from

53 the COBRA toolbox.
54
55 584

56
57
58 585 Additional file 8 (additionalFile8.xlsx): Comparison of the predicted growth phenotypes with

59
60
61
62
63
64
65

1
2
3 586 the BIOLOG PM results.

4
5 587 Additional file 9 (additionalFile9.xlsx): Reactions with changed reversibility and directionality
6
7 588 during manual curation.

8 589 Additional file 10 (additionalFile10.xlsx): Deleted metabolites during manual curation.

9
10
11 590 Additional file 11 (additionalFile11.xlsx): Deleted reactions during manual curation.

12
13
14 591 Additional file 12 (additionalFile12.xlsx): Added reactions during manual curation.

15
16
17 592 Additional file 13 (additionalFile13.xlsx): Added intermediate metabolites in GPL biosynthesis
18
19 593 pathway.

20
21
22 594 Additional file 14 (additionalFile14.xlsx): Added reactions in GPL biosynthesis pathway.

23
24
25 595 Additional file 15 (additionalFile15.xlsx): Metabolites in the constructed model *iPAO1*.

26
27
28 596 Additional file 16 (additionalFile16.xlsx): Reactions in the constructed model *iPAO1*.

29
30
31 597 Additional file 17 (additionalFile17.xlsx): Genes in the constructed model *iPAO1*.

32
33
34 598 Additional file 18 (additionalFile18.xlsx): Biomass formation formula.

35
36
37 599 Additional file 19 (additionalFile19.xlsx): Comparison of the predicted gene essentiality with
38
39 600 the information derived from two transposon insertion mutant libraries.

40
41
42 601 Additional file 20 (additionalFile20.xlsx): Metabolic flux changes in response to lipid A
43
44 602 modifications using lipidomics data as stoichiometric constraints.

45
46
47
48 603 Additional file 21 (additionalFile21.xlsx): Randomised stoichiometric coefficients of LPS
49
50 604 species.

51
52
53 605 Additional file 22 (additionalFile22.xlsx): Predicted physiochemical properties of lipid A
54
55 606 molecules.

56
57
58
59 607 Additional file 23 (additionalFile23.xlsx): Metabolic flux changes in response to lipid A
60
61
62
63
64
65

1
2
3 608 modifications with randomly assigned lipid A compositions as stoichiometric constraints.
4

5 609 Additional file 24 (additionalFile24.xlsx): Metabolic flux constraints calculated based on
6 RNA-Seq data.
7

8 611 Additional file 25 (additionalFile25.xlsx): Metabolic flux changes in response to polymyxin
9 treatment using RNA-Seq data as flux constraints.
10

11 612
12
13 613 Additional file 26 (additionalFile26.xlsx): Metabolite turnover rates.
14

15
16 614 Additional file 27 (additionalFile27.xlsx): Full names of the metabolite abbreviations in Figure
17
18 1.
19

20
21
22 616
23

24 25 617 **List of abbreviations** 26

27
28 618 2CS: two-component regulatory system; CAMHB: cation-adjusted Mueller-Hinton broth;
29

30 619 COG: clusters of orthologous groups; FBA: flux balance analysis; FDR: false discovery rate;
31

32
33 620 GC-MS: gas chromatography-mass spectrometry; GPL: Glycerolphospholipid; GPR: gene to
34

35 621 protein to reaction; GSMM: genome-scale metabolic models; IM: Inner membrane; KEGG:
36

37
38 622 Kyoto Encyclopaedia of Genes and Genomes; L-Ara4N: 4-Amino-4-deoxy-L-arabinose; LB:
39

40 623 Luria-Bertani; LC-MS: liquid chromatography-mass spectrometry; LPS: lipopolysaccharide;
41

42 624 MDR: Multidrug-resistant; OM: outer membrane; PM: Phenotypic Microarray; RPKM: Reads
43

44
45 625 Per Kilobase Million; SBML: Systems Biology Markup Language; SRA: Sequence Read
46

47 626 Archive; TCDB: Transporter Classification Database.
48
49

50 627
51

52 53 628 **Competing interests** 54

55
56 629 The authors declare no competing interest for this work.
57
58

59 630
60
61
62
63
64
65

1
2
3 **631 Funding**

4
5 **632** This study was partially supported by a Major Interdisciplinary Research Grant from Monash
6
7 **633** University and a project grant by the Australian National Health and Medical Research Council
8 **634** (NHMRC, APP1127948). J.L., T.V., and J.S. are supported by the National Institute of Allergy
9
10 **635** and Infectious Diseases of the National Institutes of Health (R01 AI111965). The content is
11
12 **636** solely the responsibility of the authors and does not necessarily represent the official views of
13
14 **637** the National Institute of Allergy and Infectious Diseases or the National Institutes of Health.
15
16 **638** T.V. is an Australian NHMRC Career Development Research Fellow. T.L. is an Australian
17
18 **639** Laureate Fellow supported by Australian Research Council. J.L. is an Australian NHMRC
19
20 **640** Senior Research Fellow.
21
22
23
24

25 **641**

26
27
28 **642 Authors' contributions**

29
30
31 **643** J.L. and F.S. conceived the project and Y.Z. developed the GSMM and conducted most
32
33 **644** analysis. T.C. and M.K. validated the model. J.Z., J.Lu and B.S. curated the model. T.V., T.L.
34
35 **645** and J.S. helped supervise the project. M.H. and M.H.M.M. provided the lipidomics and
36
37 **646** transcriptomics data, respectively.
38
39
40

41 **647**

42
43
44 **648 Acknowledgements**

45
46
47 **649** The authors acknowledge the assistance of Dr Darren Creek from the Monash Institute of
48
49 **650** Pharmaceutical Sciences in LC-MS experiments.
50
51

52
53 **651**

54
55
56 **652 References**

57
58
59
60
61
62
63
64
65

- 1
2
3
4
5
6
7
8
9
10
11
12
13
14
15
16
17
18
19
20
21
22
23
24
25
26
27
28
29
30
31
32
33
34
35
36
37
38
39
40
41
42
43
44
45
46
47
48
49
50
51
52
53
54
55
56
57
58
59
60
61
62
63
64
65
- 653 1. Scales BS, Dickson RP, LiPuma JJ and Huffnagle GB. Microbiology, genomics, and
654 clinical significance of the *Pseudomonas fluorescens* species complex, an
655 unappreciated colonizer of humans. Clin Microbiol Rev. 2014;27:927-48.
 - 656 2. Breidenstein EB, de la Fuente-Nunez C and Hancock RE. *Pseudomonas aeruginosa*:
657 all roads lead to resistance. Trends Microbiol. 2011;19:419-26.
 - 658 3. Liu YY, Wang Y, Walsh TR, Yi LX, Zhang R, Spencer J, et al. Emergence of plasmid-
659 mediated colistin resistance mechanism MCR-1 in animals and human beings in China:
660 a microbiological and molecular biological study. Lancet Infect Dis. 2016;16:161-8.
 - 661 4. Winstanley C, O'Brien S and Brockhurst MA. *Pseudomonas aeruginosa* evolutionary
662 adaptation and diversification in cystic fibrosis chronic lung infections. Trends
663 Microbiol. 2016;24:327-37.
 - 664 5. de Almeida Silva KCF, Calomino MA, Deutsch G, de Castilho SR, de Paula GR, Esper
665 LMR, et al. Molecular characterization of multidrug-resistant (MDR) *Pseudomonas*
666 *aeruginosa* isolated in a burn center. Burns. 2017;43:137-43.
 - 667 6. Church D, Elsayed S, Reid O, Winston B and Lindsay R. Burn wound infections. Clin
668 Microbiol Rev. 2006;19:403-34.
 - 669 7. Klockgether J, Cramer N, Wiehlmann L, Davenport CF and Tummeler B. *Pseudomonas*
670 *aeruginosa* genomic structure and diversity. Front Microbiol. 2011;2:150.
 - 671 8. Ramos JL and Filloux A. *Pseudomonas*: Volume 5: A model system in biology. London:
672 Springer; 2007.
 - 673 9. Nation RL, Li J, Cars O, Couet W, Dudley MN, Kaye KS, et al. Framework for
674 optimisation of the clinical use of colistin and polymyxin B: the Prato polymyxin
675 consensus. Lancet Infect Dis. 2015;15:225-34.

- 676 10. Pedersen MG, Jensen-Fangel S, Olesen HV, Nørskov-Lauritsen N and Wang M. 129
1
2 677 Colistin resistance in *Achromobacter* sp. and *Pseudomonas aeruginosa* isolated from
3
4 678 Danish cystic fibrosis patients is not related to plasmid-mediated expression of *mcr-1*.
5
6
7 679 J Cyst Fibros. 2017;16:S98.
8
9
10 680 11. Wi YM, Choi JY, Lee JY, Kang CI, Chung DR, Peck KR, et al. Emergence of colistin
11
12 681 resistance in *Pseudomonas aeruginosa* ST235 clone in South Korea. Int J Antimicrob
13
14 682 Agents. 2017;49:767-9.
15
16
17
18 683 12. Yu Z, Qin W, Lin J, Fang S and Qiu J. Antibacterial mechanisms of polymyxin and
19
20 684 bacterial resistance. Biomed Res Int. 2015;2015:679109-19.
21
22
23 685 13. Trimble MJ, Mlynarcik P, Kolar M and Hancock RE. Polymyxin: alternative
24
25 686 mechanisms of action and resistance. Cold Spring Harb Perspect Med. 2016;6:a025288.
26
27
28 687 14. Han M, Zhu Y, Cheah SE, Johnson MD, Yu H, Shen HH, et al. Polymyxin resistance
29
30 688 in *Pseudomonas aeruginosa*: metabolomic changes underpin lipid A modifications. In:
31
32 689 *ASM Microbe 2017* Boston, USA, 2016, p.491.
33
34
35
36 690 15. Hussein MH, Maifiah MHM, Han M, Tran TB, Zhu Y, Hancock REW, et al.
37
38 691 Mechanisms of synergistic killing against *Pseudomonas aeruginosa* by polymyxin B
39
40 692 and amikacin: A metabolomics study. In: *European Congress of Clinical Microbiology*
41
42 693 *and Infectious Diseases* Vienna, Austria, 2017, p.EV0387. ESCMID.
43
44
45
46 694 16. O'Brien EJ, Monk JM and Palsson BO. Using genome-scale models to predict
47
48 695 biological capabilities. Cell. 2015;161:971-87.
49
50
51
52 696 17. Hohenschuh W, Hector R and Murthy GS. A dynamic flux balance model and
53
54 697 bottleneck identification of glucose, xylose, xylulose co-fermentation in
55
56 698 *Saccharomyces cerevisiae*. Bioresour Technol. 2015;188:153-60.
57
58
59
60
61
62
63
64
65

- 699 18. Hanly TJ and Henson MA. Dynamic metabolic modeling of a microaerobic yeast co-
1
2 700 culture: predicting and optimizing ethanol production from glucose/xylose mixtures.
3
4 701 Biotechnol Biofuels. 2013;6:44.
5
6
7 702 19. Hanly TJ and Henson MA. Dynamic flux balance modeling of microbial co-cultures
8
9 703 for efficient batch fermentation of glucose and xylose mixtures. Biotechnol Bioeng.
10
11 704 2011;108:376-85.
12
13
14 705 20. Bosi E, Monk JM, Aziz RK, Fondi M, Nizet V and Palsson BO. Comparative genome-
15
16 706 scale modelling of *Staphylococcus aureus* strains identifies strain-specific metabolic
17
18 707 capabilities linked to pathogenicity. Proc Natl Acad Sci U S A. 2016;113:E3801-9.
19
20
21 708 21. Kim HU, Kim SY, Jeong H, Kim TY, Kim JJ, Choy HE, et al. Integrative genome-scale
22
23 709 metabolic analysis of *Vibrio vulnificus* for drug targeting and discovery. Mol Syst Biol.
24
25 710 2011;7:460.
26
27
28 711 22. Krueger AS, Munck C, Dantas G, Church GM, Galagan J, Lehar J, et al. Simulating
29
30 712 serial-target antibacterial drug synergies using flux balance analysis. PLoS One.
31
32 713 2016;11:e0147651.
33
34
35 714 23. Aziz RK, Monk JM, Lewis RM, In Loh S, Mishra A, Abhay Nagle A, et al. Systems
36
37 715 biology-guided identification of synthetic lethal gene pairs and its potential use to
38
39 716 discover antibiotic combinations. Scientific reports. 2015;5:16025.
40
41
42 717 24. Bordbar A, Monk JM, King ZA and Palsson BO. Constraint-based models predict
43
44 718 metabolic and associated cellular functions. Nat Rev Genet. 2014;15:107-20.
45
46
47 719 25. Oberhardt MA, Puchalka J, Fryer KE, Martins dos Santos VA and Papin JA. Genome-
48
49 720 scale metabolic network analysis of the opportunistic pathogen *Pseudomonas*
50
51 721 *aeruginosa* PAO1. J Bacteriol. 2008;190:2790-803.
52
53
54
55
56
57
58
59
60
61
62
63
64
65

- 1
2
3
4
5
6
7
8
9
10
11
12
13
14
15
16
17
18
19
20
21
22
23
24
25
26
27
28
29
30
31
32
33
34
35
36
37
38
39
40
41
42
43
44
45
46
47
48
49
50
51
52
53
54
55
56
57
58
59
60
61
62
63
64
65
- 722 26. Henry CS, DeJongh M, Best AA, Frybarger PM, Linsay B and Stevens RL. High-
723 throughput generation, optimization and analysis of genome-scale metabolic models.
724 Nat Biotechnol. 2010;28:977-82.
- 725 27. Oberhardt MA, Puchalka J, Martins dos Santos VA and Papin JA. Reconciliation of
726 genome-scale metabolic reconstructions for comparative systems analysis. PLoS
727 Comput Biol. 2011;7:e1001116.
- 728 28. Bartell JA, Blazier AS, Yen P, Thogersen JC, Jelsbak L, Goldberg JB, et al.
729 Reconstruction of the metabolic network of *Pseudomonas aeruginosa* to interrogate
730 virulence factor synthesis. Nat Commun. 2017;8:14631.
- 731 29. Devoid S, Overbeek R, DeJongh M, Vonstein V, Best AA and Henry C. Automated
732 genome annotation and metabolic model reconstruction in the SEED and Model SEED.
733 Methods Mol Biol. 2013;985:17-45.
- 734 30. Oberhardt MA, Goldberg JB, Hogardt M and Papin JA. Metabolic network analysis of
735 *Pseudomonas aeruginosa* during chronic cystic fibrosis lung infection. J Bacteriol.
736 2010;192:5534-48.
- 737 31. Biggs MB and Papin JA. Novel multiscale modeling tool applied to *Pseudomonas*
738 *aeruginosa* biofilm formation. PLoS One. 2013;8:e78011.
- 739 32. Vital-Lopez FG, Reifman J and Wallqvist A. Biofilm formation mechanisms of
740 *Pseudomonas aeruginosa* predicted via genome-scale kinetic models of bacterial
741 metabolism. PLoS Comput Biol. 2015;11:e1004452.
- 742 33. Sigurdsson G, Fleming RM, Heinken A and Thiele I. A systems biology approach to
743 drug targets in *Pseudomonas aeruginosa* biofilm. PLoS One. 2012;7:e34337.
- 744 34. Xu Z, Fang X, Wood TK and Huang ZJ. A systems-level approach for investigating
745 *Pseudomonas aeruginosa* biofilm formation. PLoS One. 2013;8:e57050.

- 1
2
3
4
5
6
7
8
9
10
11
12
13
14
15
16
17
18
19
20
21
22
23
24
25
26
27
28
29
30
31
32
33
34
35
36
37
38
39
40
41
42
43
44
45
46
47
48
49
50
51
52
53
54
55
56
57
58
59
60
61
62
63
64
65
- 746 35. Perumal D, Samal A, Sakharkar KR and Sakharkar MK. Targeting multiple targets in
747 *Pseudomonas aeruginosa* PAO1 using flux balance analysis of a reconstructed
748 genome-scale metabolic network. *J Drug Target*. 2011;19:1-13.
- 749 36. Dalebroux ZD, Matamouros S, Whittington D, Bishop RE and Miller SI. PhoPQ
750 regulates acidic glycerophospholipid content of the *Salmonella Typhimurium* outer
751 membrane. *Proc Natl Acad Sci U S A*. 2014;111:1963-8.
- 752 37. Raetz CR, Reynolds CM, Trent MS and Bishop RE. Lipid A modification systems in
753 Gram-negative bacteria. *Annu Rev Biochem*. 2007;76:295-329.
- 754 38. Maifiah MH, Creek DJ, Nation RL, Forrest A, Tsuji BT, Velkov T, et al. Untargeted
755 metabolomics analysis reveals key pathways responsible for the synergistic killing of
756 colistin and doripenem combination against *Acinetobacter baumannii*. *Sci Rep*.
757 2017;7:45527.
- 758 39. Han ML, Zhu Y, Cheah S-E, Johnson MD, Yu HH, Maifiah MHM, et al. Polymyxin
759 resistance due to mutations in *pmrB* caused global metabolomics changes in
760 *Pseudomonas aeruginosa*. In: *The Australian & New Zealand Metabolomics*
761 *Conference* Melbourne, Australia, 30 March 2016, p.106.
- 762 40. Frimmersdorf E, Horatzek S, Pelnikevich A, Wiehlmann L and Schomburg D. How
763 *Pseudomonas aeruginosa* adapts to various environments: a metabolomic approach.
764 *Environ Microbiol*. 2010;12:1734-47.
- 765 41. Kanehisa M, Sato Y, Kawashima M, Furumichi M and Tanabe M. KEGG as a reference
766 resource for gene and protein annotation. *Nucleic Acids Res*. 2016;44:D457-62.
- 767 42. Caspi R, Billington R, Ferrer L, Foerster H, Fulcher CA, Keseler IM, et al. The
768 MetaCyc database of metabolic pathways and enzymes and the BioCyc collection of
769 pathway/genome databases. *Nucleic Acids Res*. 2016;44:D471-80.

- 1
2
3
4
5
6
7
8
9
10
11
12
13
14
15
16
17
18
19
20
21
22
23
24
25
26
27
28
29
30
31
32
33
34
35
36
37
38
39
40
41
42
43
44
45
46
47
48
49
50
51
52
53
54
55
56
57
58
59
60
61
62
63
64
65
- 770 43. Saier MH, Jr., Reddy VS, Tsu BV, Ahmed MS, Li C and Moreno-Hagelsieb G. The
771 Transporter Classification Database (TCDB): recent advances. *Nucleic Acids Res.*
772 2016;44:D372-9.
- 773 44. Elbourne LD, Tetu SG, Hassan KA and Paulsen IT. TransportDB 2.0: a database for
774 exploring membrane transporters in sequenced genomes from all domains of life.
775 *Nucleic Acids Res.* 2017;45:D320-D4.
- 776 45. Winsor GL, Griffiths EJ, Lo R, Dhillon BK, Shay JA and Brinkman FS. Enhanced
777 annotations and features for comparing thousands of *Pseudomonas* genomes in the
778 *Pseudomonas* genome database. *Nucleic Acids Res.* 2016;44:D646-53.
- 779 46. Lewenza S, Falsafi RK, Winsor G, Gooderham WJ, McPhee JB, Brinkman FS, et al.
780 Construction of a mini-Tn5-*luxCDABE* mutant library in *Pseudomonas aeruginosa*
781 PAO1: a tool for identifying differentially regulated genes. *Genome Res.* 2005;15:583-
782 9.
- 783 47. Held K, Ramage E, Jacobs M, Gallagher L and Manoil C. Sequence-verified two-allele
784 transposon mutant library for *Pseudomonas aeruginosa* PAO1. *J Bacteriol.*
785 2012;194:6387-9.
- 786 48. Maifiah MHM. *Deciphering the modes of action of polymyxins and the synergistic*
787 *combinations against multidrug-resistant Gram-negative bacteria: a systems*
788 *pharmacology approach.* PhD thesis, Monash University, Australia, 2017.
- 789 49. Liao Y, Smyth GK and Shi W. The Subread aligner: fast, accurate and scalable read
790 mapping by seed-and-vote. *Nucleic Acids Res.* 2013;41:e108.
- 791 50. Powell D: Degust. <http://degust.erc.monash.edu/> (2017). Accessed Oct 18 2017.

- 1
2
3
4
5
6
7
8
9
10
11
12
13
14
15
16
17
18
19
20
21
22
23
24
25
26
27
28
29
30
31
32
33
34
35
36
37
38
39
40
41
42
43
44
45
46
47
48
49
50
51
52
53
54
55
56
57
58
59
60
61
62
63
64
65
- 792 51. Creek DJ, Jankevics A, Burgess KE, Breitling R and Barrett MP. IDEOM: an Excel
793 interface for analysis of LC-MS-based metabolomics data. *Bioinformatics*.
794 2012;28:1048-9.
- 795 52. Satish Kumar V, Dasika MS and Maranas CD. Optimization based automated curation
796 of metabolic reconstructions. *BMC Bioinformatics*. 2007;8:212.
- 797 53. Finn RD, Coghill P, Eberhardt RY, Eddy SR, Mistry J, Mitchell AL, et al. The Pfam
798 protein families database: towards a more sustainable future. *Nucleic Acids Res*.
799 2016;44:D279-85.
- 800 54. Zdobnov EM, Tegenfeldt F, Kuznetsov D, Waterhouse RM, Simao FA, Ioannidis P, et
801 al. OrthoDB v9.1: cataloging evolutionary and functional annotations for animal,
802 fungal, plant, archaeal, bacterial and viral orthologs. *Nucleic Acids Res*. 2017;45:D744-
803 D9.
- 804 55. Hempel N, Görisch H and Mern DS. Gene *erca*, encoding a putative iron-containing
805 alcohol dehydrogenase, is involved in regulation of ethanol utilization in *Pseudomonas*
806 *aeruginosa*. *J Bacteriol*. 2013;195:3925-32.
- 807 56. Kohanski MA, Dwyer DJ and Collins JJ. How antibiotics kill bacteria: from targets to
808 networks. *Nat Rev Microbiol*. 2010;8:423-35.
- 809 57. Typas A, Banzhaf M, Gross CA and Vollmer W. From the regulation of peptidoglycan
810 synthesis to bacterial growth and morphology. *Nat Rev Microbiol*. 2011;10:123-36.
- 811 58. Cox E, Michalak A, Pagentine S, Seaton P and Pokorny A. Lysylated phospholipids
812 stabilize models of bacterial lipid bilayers and protect against antimicrobial peptides.
813 *Biochim Biophys Acta*. 2014;1838:2198-204.

- 1
2
3
4
5
6
7
8
9
10
11
12
13
14
15
16
17
18
19
20
21
22
23
24
25
26
27
28
29
30
31
32
33
34
35
36
37
38
39
40
41
42
43
44
45
46
47
48
49
50
51
52
53
54
55
56
57
58
59
60
61
62
63
64
65
- 814 59. Kondakova T, D'Heygere F, Feuilloley MJ, Orange N, Heipieper HJ and Duclairoir Poc
815 C. Glycerophospholipid synthesis and functions in *Pseudomonas*. Chem Phys Lipids.
816 2015;190:27-42.
- 817 60. Velkov T, Thompson PE, Nation RL and Li J. Structure–activity relationships of
818 polymyxin antibiotics. J Med Chem. 2010;53:1898-916.
- 819 61. Kim S, Thiessen PA, Bolton EE, Chen J, Fu G, Gindulyte A, et al. PubChem Substance
820 and Compound databases. Nucleic Acids Res. 2016;44:D1202-13.
- 821 62. Pence HE and Williams A. ChemSpider: an online chemical information resource. J
822 Chem Educ. 2010;87:1123-4.
- 823 63. Hastings J, de Matos P, Dekker A, Ennis M, Harsha B, Kale N, et al. The ChEBI
824 reference database and ontology for biologically relevant chemistry: enhancements for
825 2013. Nucleic Acids Res. 2013;41:D456-63.
- 826 64. King ZA, Lu J, Drager A, Miller P, Federowicz S, Lerman JA, et al. BiGG Models: A
827 platform for integrating, standardizing and sharing genome-scale models. Nucleic
828 Acids Res. 2016;44:D515-22.
- 829 65. Jacobs MA, Alwood A, Thaipisuttikul I, Spencer D, Haugen E, Ernst S, et al.
830 Comprehensive transposon mutant library of *Pseudomonas aeruginosa*. Proc Natl Acad
831 Sci U S A. 2003;100:14339-44.
- 832 66. Olaitan AO, Morand S and Rolain JM. Mechanisms of polymyxin resistance: acquired
833 and intrinsic resistance in bacteria. Front Microbiol. 2014;5:643.
- 834 67. Graham LL, Beveridge TJ and Nanninga N. Periplasmic space and the concept of the
835 periplasm. Trends Biochem Sci. 1991;16:328-9.

- 1
2
3
4
5
6
7
8
9
10
11
12
13
14
15
16
17
18
19
20
21
22
23
24
25
26
27
28
29
30
31
32
33
34
35
36
37
38
39
40
41
42
43
44
45
46
47
48
49
50
51
52
53
54
55
56
57
58
59
60
61
62
63
64
65
- 836 68. Silhavy TJ, Kahne D and Walker S. The bacterial cell envelope. Cold Spring Harb
837 Perspect Biol. 2010;2:a000414.
- 838 69. Han M, Shen HH, Zhu Y, Roberts KD, Le Brun AP, Moskowitz SM, et al. Deciphering
839 the mechanisms of polymyxin resistance in *Pseudomonas aeruginosa*: A systems
840 pharmacology and neutron reflectometry approach. In: *Solutions for Drug-Resistant*
841 *Infections (SDRI) 2017* Brisbane, Australia, 3-5, April 2017, p.P23. SDRI 2017.
- 842 70. Maifiah MH, Cheah SE, Johnson MD, Han ML, Boyce JD, Thamlikitkul V, et al.
843 Global metabolic analyses identify key differences in metabolite levels between
844 polymyxin-susceptible and polymyxin-resistant *Acinetobacter baumannii*. *Sci Rep.*
845 2016;6:22287.
- 846 71. Henry R, Crane B, Powell D, Deveson Lucas D, Li Z, Aranda J, et al. The
847 transcriptomic response of *Acinetobacter baumannii* to colistin and doripenem alone
848 and in combination in an *in vitro* pharmacokinetics/pharmacodynamics model. *J*
849 *Antimicrob Chemother.* 2015;70:1303-13.
- 850 72. Abdul Rahim N, Cheah S, Zhu Y, Johnson M, Boyce J, Yu H, et al. Integrative multi-
851 omics network analysis of the synergistic killing of polymyxin B and chloramphenicol
852 combination against an NDM-producing *Klebsiella pneumoniae* isolate. In: *2016*
853 *European Congress of Clinical Microbiology and Infectious Diseases (ECCMID)*
854 *Amsterdam, Netherland, 2016*, p.EV0651. ESCMID.
- 855 73. Machado D and Herrgard M. Systematic evaluation of methods for integration of
856 transcriptomic data into constraint-based models of metabolism. *PLoS Comput Biol.*
857 2014;10:e1003580.

- 1
2
3
4
5
6
7
8
9
10
11
12
13
14
15
16
17
18
19
20
21
22
23
24
25
26
27
28
29
30
31
32
33
34
35
36
37
38
39
40
41
42
43
44
45
46
47
48
49
50
51
52
53
54
55
56
57
58
59
60
61
62
63
64
65
- 858 74. Colijn C, Brandes A, Zucker J, Lun DS, Weiner B, Farhat MR, et al. Interpreting
859 expression data with metabolic flux models: predicting *Mycobacterium tuberculosis*
860 mycolic acid production. PLoS Comput Biol. 2009;5:e1000489.
- 861 75. Blazier AS and Papin JA. Integration of expression data in genome-scale metabolic
862 network reconstructions. Front Physiol. 2012;3:299.
- 863 76. Kohanski MA, Dwyer DJ, Hayete B, Lawrence CA and Collins JJ. A common
864 mechanism of cellular death induced by bactericidal antibiotics. Cell. 2007;130:797-
865 810.
- 866 77. Johnson L, Mulcahy H, Kanevets U, Shi Y and Lewenza S. Surface-localized
867 spermidine protects the *Pseudomonas aeruginosa* outer membrane from antibiotic
868 treatment and oxidative stress. J Bacteriol. 2012;194:813-26.
- 869 78. Fernandez L, Jenssen H, Bains M, Wiegand I, Gooderham WJ and Hancock RE. The
870 two-component system CprRS senses cationic peptides and triggers adaptive resistance
871 in *Pseudomonas aeruginosa* independently of ParRS. Antimicrob Agents Chemother.
872 2012;56:6212-22.
- 873 79. Barrow K and Kwon DH. Alterations in two-component regulatory systems of *phoPQ*
874 and *pmrAB* are associated with polymyxin B resistance in clinical isolates of
875 *Pseudomonas aeruginosa*. Antimicrob Agents Chemother. 2009;53:5150-4.
- 876 80. Owusu-Anim D and Kwon DH. Differential role of two-component regulatory systems
877 (*phoPQ* and *pmrAB*) in polymyxin B susceptibility of *Pseudomonas aeruginosa*. Adv
878 Microbiol. 2012;2:31-6.
- 879 81. Moskowitz SM, Ernst RK and Miller SI. PmrAB, a two-component regulatory system
880 of *Pseudomonas aeruginosa* that modulates resistance to cationic antimicrobial
881 peptides and addition of aminoarabinose to lipid A. J Bacteriol. 2004;186:575-9.

- 1
2
3
4
5
6
7
8
9
10
11
12
13
14
15
16
17
18
19
20
21
22
23
24
25
26
27
28
29
30
31
32
33
34
35
36
37
38
39
40
41
42
43
44
45
46
47
48
49
50
51
52
53
54
55
56
57
58
59
60
61
62
63
64
65
- 882 82. Gutu AD, Sgambati N, Strasbourger P, Brannon MK, Jacobs MA, Haugen E, et al.
883 Polymyxin resistance of *Pseudomonas aeruginosa* *phoQ* mutants is dependent on
884 additional two-component regulatory systems. *Antimicrob Agents Chemother.*
885 2013;57:2204-15.
- 886 83. Winfield MD and Groisman EA. Phenotypic differences between *Salmonella* and
887 *Escherichia coli* resulting from the disparate regulation of homologous genes. *Proc Natl*
888 *Acad Sci U S A.* 2004;101:17162-7.
- 889 84. McPhee JB, Bains M, Winsor G, Lewenza S, Kwasnicka A, Brazas MD, et al.
890 Contribution of the PhoP-PhoQ and PmrA-PmrB two-component regulatory systems to
891 Mg²⁺-induced gene regulation in *Pseudomonas aeruginosa*. *J Bacteriol.*
892 2006;188:3995-4006.
- 893 85. Thaipisuttikul I, Hittle LE, Chandra R, Zangari D, Dixon CL, Garrett TA, et al. A
894 divergent *Pseudomonas aeruginosa* palmitoyltransferase essential for cystic fibrosis-
895 specific lipid A. *Mol Microbiol.* 2014;91:158-74.
- 896 86. Fernández L, Gooderham WJ, Bains M, McPhee JB, Wiegand I and Hancock REW.
897 Adaptive resistance to the “last hope” antibiotics polymyxin B and colistin in
898 *Pseudomonas aeruginosa* is mediated by the novel two-component regulatory system
899 ParR-ParS. *Antimicrobial Agents and Chemotherapy.* 2010;54:3372-82.
- 900 87. Thiele I and Palsson BO. A protocol for generating a high-quality genome-scale
901 metabolic reconstruction. *Nat Protoc.* 2010;5:93-121.
- 902 88. Yu NY, Wagner JR, Laird MR, Melli G, Rey S, Lo R, et al. PSORTb 3.0: improved
903 protein subcellular localization prediction with refined localization subcategories and
904 predictive capabilities for all prokaryotes. *Bioinformatics.* 2010;26:1608-15.

- 1
2
3
4
5
6
7
8
9
10
11
12
13
14
15
16
17
18
19
20
21
22
23
24
25
26
27
28
29
30
31
32
33
34
35
36
37
38
39
40
41
42
43
44
45
46
47
48
49
50
51
52
53
54
55
56
57
58
59
60
61
62
63
64
65
- 905 89. Hucka M, Finney A, Sauro HM, Bolouri H, Doyle JC, Kitano H, et al. The systems
906 biology markup language (SBML): a medium for representation and exchange of
907 biochemical network models. *Bioinformatics*. 2003;19:524-31.
- 908 90. Hucka M and Finney AM: Systems Biology Markup Language (SBML) Level 2:
909 Structures and Facilities for Model Definitions.
910 <http://identifiers.org/combine.specifications/sbml.level-2.version-1> (2003). Accessed
911 Oct 18 2017.
- 912 91. Rohn H, Junker A, Hartmann A, Grafahrend-Belau E, Treutler H, Klapperstuck M, et
913 al. VANTED v2: a framework for systems biology applications. *BMC Syst Biol*.
914 2012;6:139.
- 915 92. Schellenberger J, Que R, Fleming RM, Thiele I, Orth JD, Feist AM, et al. Quantitative
916 prediction of cellular metabolism with constraint-based models: the COBRA Toolbox
917 v2.0. *Nat Protoc*. 2011;6:1290-307.
- 918 93. Moskowitz SM, Brannon MK, Dasgupta N, Pier M, Sgambati N, Miller AK, et al. PmrB
919 mutations promote polymyxin resistance of *Pseudomonas aeruginosa* isolated from
920 colistin-treated cystic fibrosis patients. *Antimicrob Agents Chemother*. 2012;56:1019-
921 30.
- 922 94. Saa PA and Nielsen LK. ll-ACHRB: a scalable algorithm for sampling the feasible
923 solution space of metabolic networks. *Bioinformatics*. 2016;32:2330-7.
- 924 95. Mo ML, Palsson BO and Herrgard MJ. Connecting extracellular metabolomic
925 measurements to intracellular flux states in yeast. *BMC Syst Biol*. 2009;3:37.
- 926 96. McCarthy DJ, Chen Y and Smyth GK. Differential expression analysis of multifactor
927 RNA-Seq experiments with respect to biological variation. *Nucleic Acids Res*.
928 2012;40:4288-97.

929 97. Kim PJ, Lee DY, Kim TY, Lee KH, Jeong H, Lee SY, et al. Metabolite essentiality
1
2 930 elucidates robustness of *Escherichia coli* metabolism. Proc Natl Acad Sci U S A.
3
4
5 931 2007;104:13638-42.
6

7
8 932 98. Benjamini Y and Hochberg Y. Controlling the false discovery rate: A practical and
9
10 933 powerful approach to multiple testing. J Roy Stat Soc B Met. 1995;57:289-300.
11

12
13 934

14
15
16 935 **Figure legends**
17

18
19 936 **Figure 1.** The curated GPL biosynthesis in *iPAO1*. [c], intracellular metabolites; [p],
20
21 937 periplasmic metabolites; [e], external metabolites. Blue arrows indicate transport reactions.
22
23 938 Full names of metabolite classes are listed in **Additional file 27**.

24
25
26 939 **Figure 2.** LPS biosynthesis and modification in *iPAO1*. (A) VANTED diagram showing the
27
28 940 biosynthesis of different LPS molecules. (B) LPS biosynthesis pathway; lipid A and LPS are
29
30 941 indicated in the same colour as in (A).
31
32

33
34 942 **Figure 3.** Constitutional genes, reactions and metabolites in *iPAO1*. (A) Sources of *iPAO1*
35
36 943 components. (B) Radar map showing the percentages of metabolites and reactions with valid
37
38 944 database identifiers. (C) The COG functional classification of the involved genes in iMO1056,
39
40 945 Opt208964 and *iPAO1*. Percentages given in the middle indicate the coverages of COG groups.
41
42 946 The proportions of the curated reactions (D), reaction-to-gene ratio (E) and predicted
43
44 947 subcellular localisations of the involved proteins (F) are shown for each pathway or COG group.
45
46 948 In panel D, red bars indicate the curated reactions; whereas blue bars indicate the reactions
47
48 949 from previous model. In panel D and E, pathways with the highest curation proportion or
49
50 950 reaction-to-gene ratio are highlighted in red.
51
52

53
54
55 951 **Figure 4.** Comparison of the BIOLOG result (left columns) and model prediction (right
56
57 952 columns). Blue indicates growth; whereas yellow indicates no growth.
58
59
60
61
62
63
64
65

953 **Figure 5.** Simulation of the impact of lipid A modifications on bacterial growth, metabolism
 954 and OM physiochemical properties. The significant correlation ($P<0.05$) of paired items is
 955 indicated in red.

956 **Figure 6.** Polymyxin B induced metabolic perturbations. The distributions of metabolic fluxes
 957 and metabolite turnover rates are shown in subgraphs with red indicating control and blue
 958 indicating polymyxin B treatment.

959

960 **Tables and their legends**

961 **Table 1.** Components in model iMO1056, Opt208964 and iPAO1.

	<i>iPAO1</i>	<i>iMO1056</i>	<i>Opt208964</i>
Genes	1,458	1,042	1,021
Reactions	4,365	992	1,609
Cytoplasmic metabolic reactions	1,716	730	1,132
Periplasmic metabolic reactions	403	0	0
External metabolic reactions	40	0	0
Transport reactions	960	150	253
Transport across IM	519	0	0
Transport across OM	441	0	0
Transport from cytoplasm to extracellular space	0	150	253
Boundary reactions	352	112	223

	Reactions without associated genes	628	159	374
	Sink reactions	0	0	1
Metabolites		3,022	858	1,344
	Cytosol	1,519	746	1,121
	Periplasm	698	0	0
	Extracellular space	805	112	223
Pathways		109	- ^a	117

^a Pathway information is not available in iMO1056 from the Model SEED database.

Table 2. Lipid A composition (%) in the outer leaflet of the OM in PAO1 [14].

Lipid A species	Control	Polymyxin B treated
Hexa-lipid A	42.5±0.46	11.7±1.13
Penta-lipid A	57.5±0.46	67.7±3.16
L-Aminoarabinosylated hexa-LA	0	1.24±0.31
L-Aminoarabinosylated penta-LA	0	19.4±3.44
Total	100	100

Table 3. Specific growth rate, significantly altered major exchange fluxes (>1 mmol·gDW·h⁻¹), respiration quotient and the fluxes through F₀F₁-ATPase calculated using the RNA-Seq data [48] as flux constraints.

Exchange flux (mmol·gDW·h ⁻¹)	Control	Polymyxin B treatment	Z-score	FDR ^a
--	---------	--------------------------	---------	------------------

1	Specific growth rate (h ⁻¹)	0.82±0.00	0.67±0.00	10,201.3	0.00
2					
3	H ₂ O	46.9±21.8	53.0±19.0	20.37	0.00
4					
5	O ₂	-106.0±23.0	-113.4±19.8	24.30	0.00
6					
7					
8	CO ₂	109.2±22.6	115.8±19.3	22.62	0.00
9					
10					
11	NH ₄ ⁺	36.6±9.29	38.0±8.77	10.94	0.00
12					
13					
14	Glycine	2.15±4.76	1.92±4.46	3.05	0.00
15					
16					
17	L-Alanine	1.21±5.01	-0.52±2.20	31.77	0.00
18					
19					
20	Succinate	2.08±4.19	2.52±4.42	7.27	0.00
21					
22					
23	H ⁺	-41.5±14.1	-40.4±11.9	6.44	0.00
24					
25					
26	Methanethiol	1.53±0.82	1.34±1.11	12.62	0.00
27					
28					
29	H ₂ S	1.66±1.74	1.41±2.18	9.29	0.00
30					
31					
32	Respiration Quotient (RQ)	1.03±0.10	1.02±0.10	7.63	0.00
33					
34					
35	ATPase (mmol·gDW·h ⁻¹)	-188.6±52.4	-167.6±48.4	29.62	0.00
36					
37					

^a FDR was calculated using the Benjamini-Hochberg method [98].

968

969

1
2
3
4
5
6
7
8
9
10
11
12
13
14
15
16
17
18
19
20
21
22
23
24
25
26
27
28
29
30
31
32
33
34
35
36
37
38
39
40
41
42
43
44
45
46
47
48
49
50
51
52
53
54
55
56
57
58
59
60
61
62
63
64
65

Figure 1

[Click here to download Figure 1.eps](#)

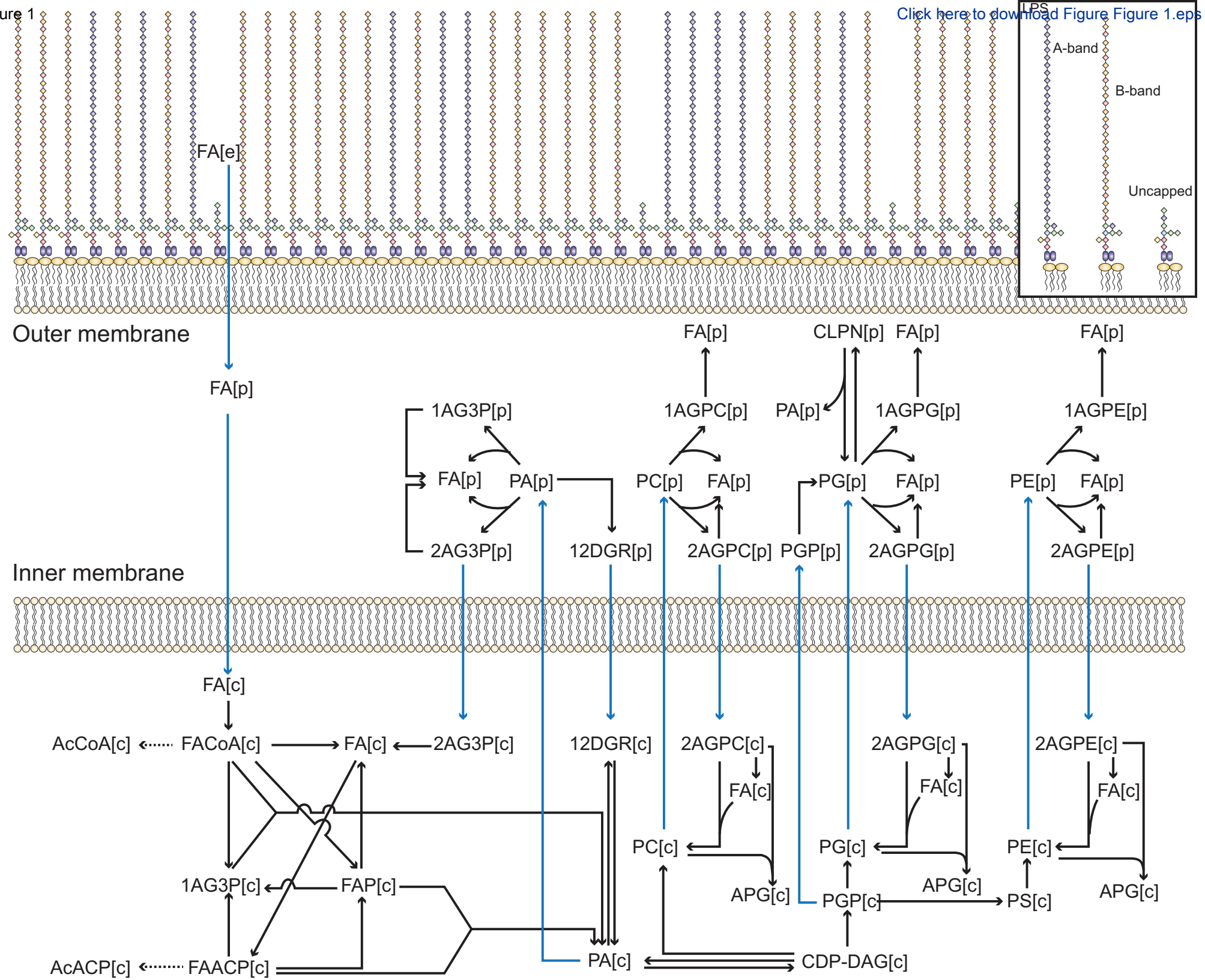
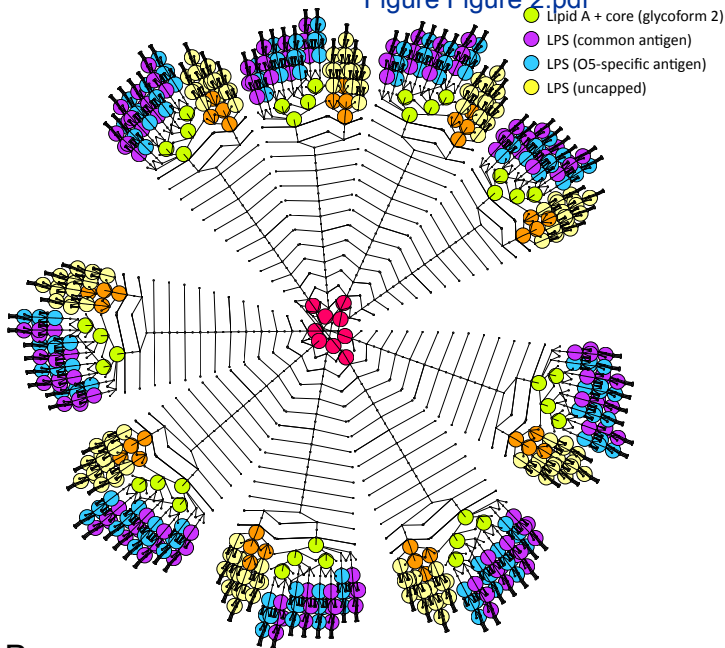
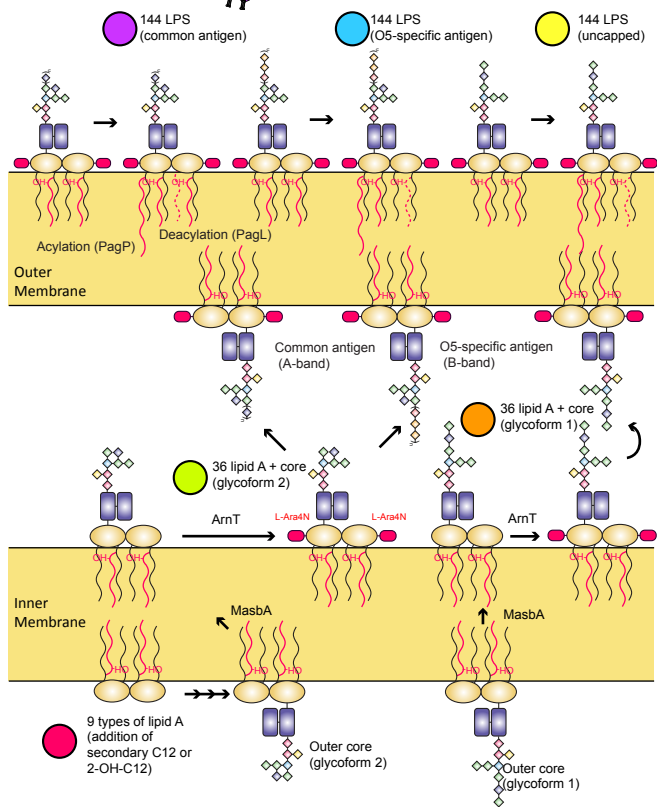


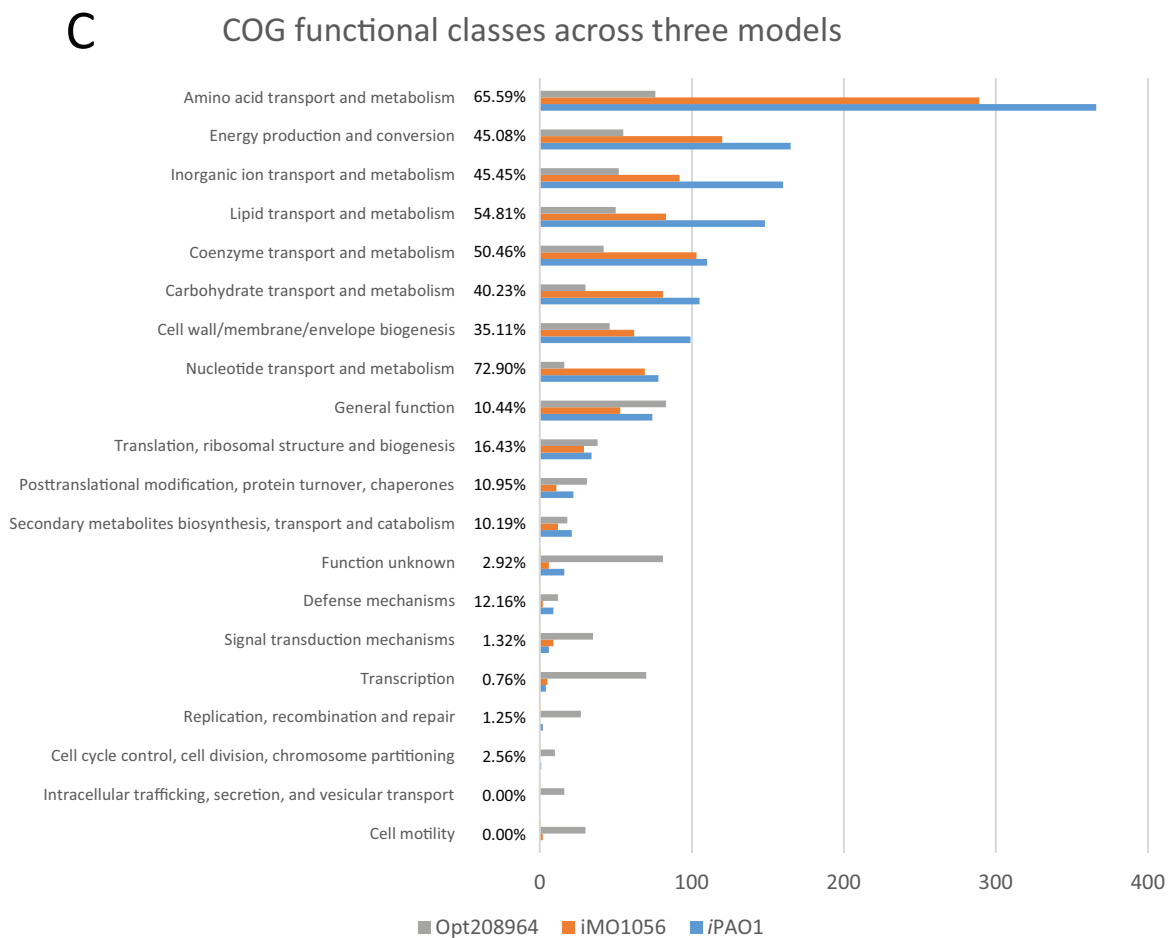
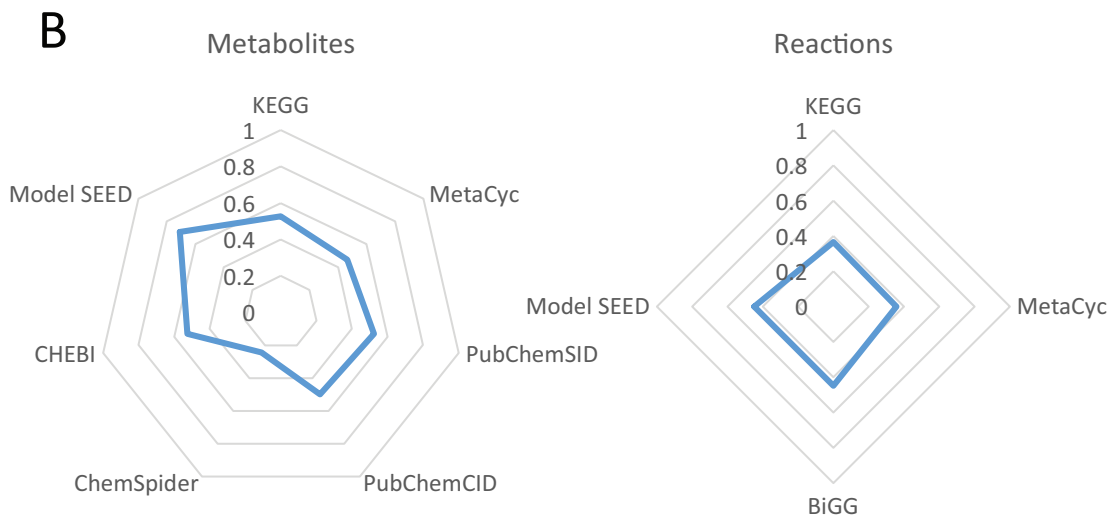
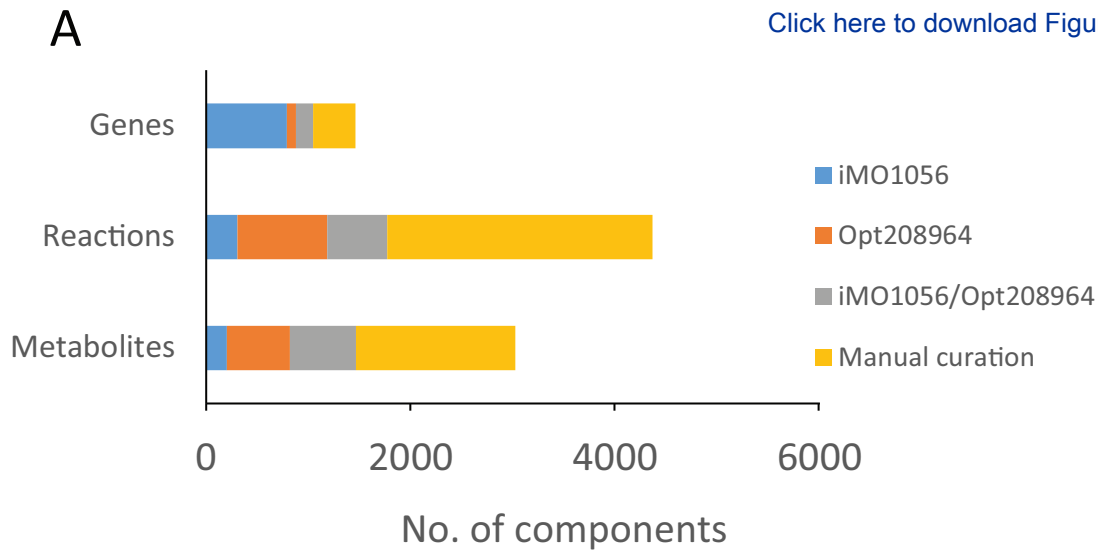
Figure 2

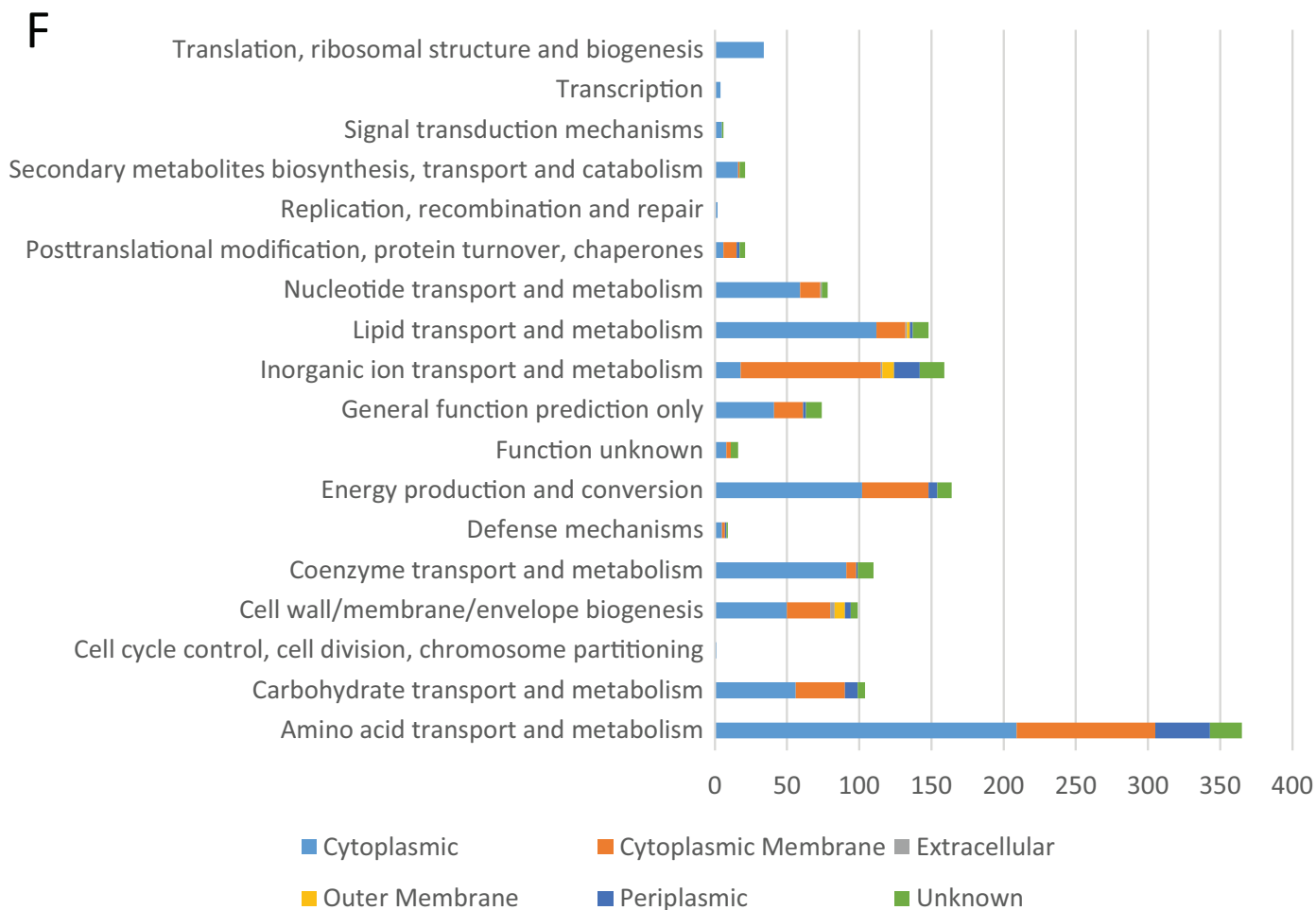
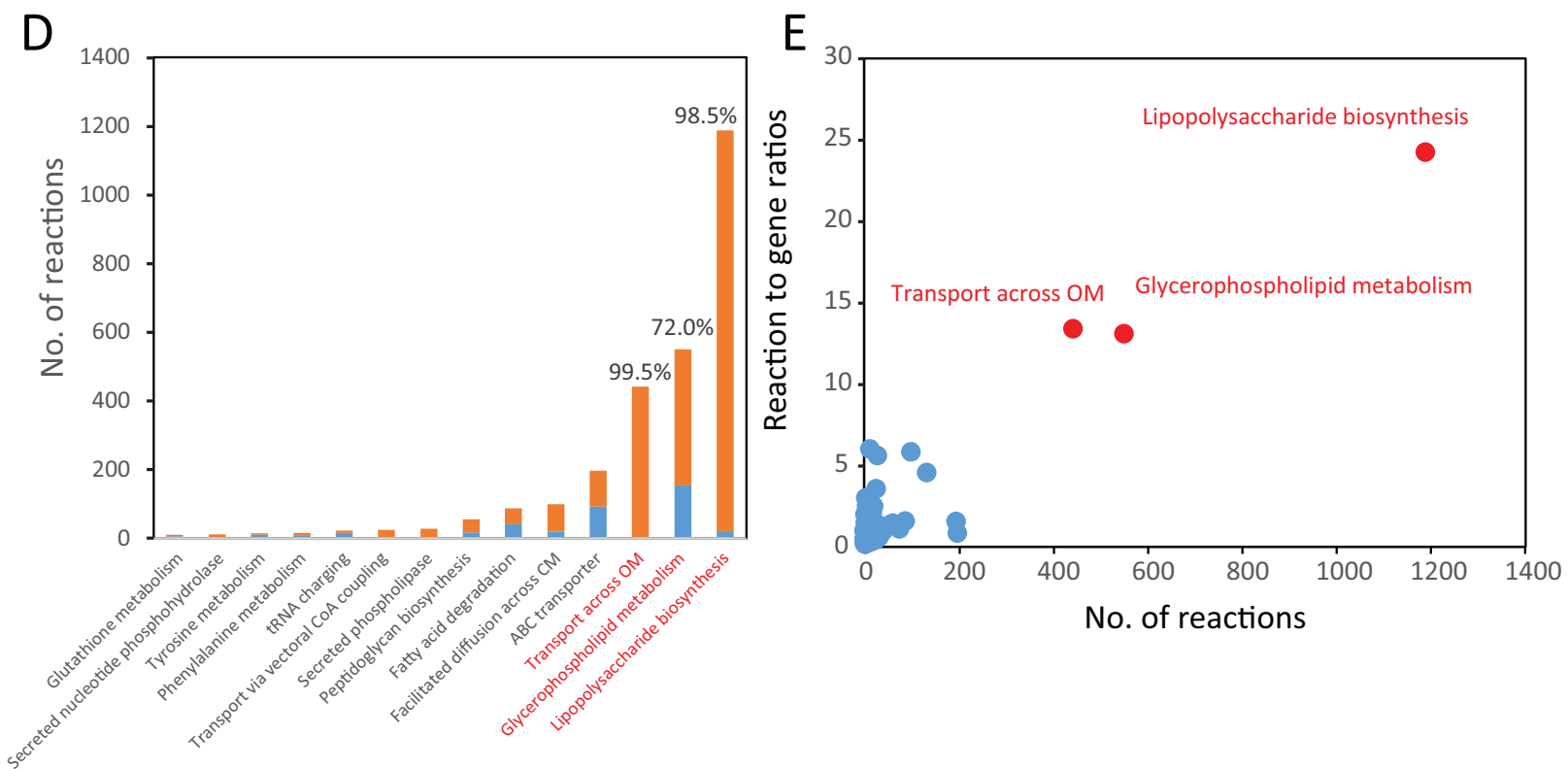
[Click here to download Figure Figure 2.pdf](#)



B

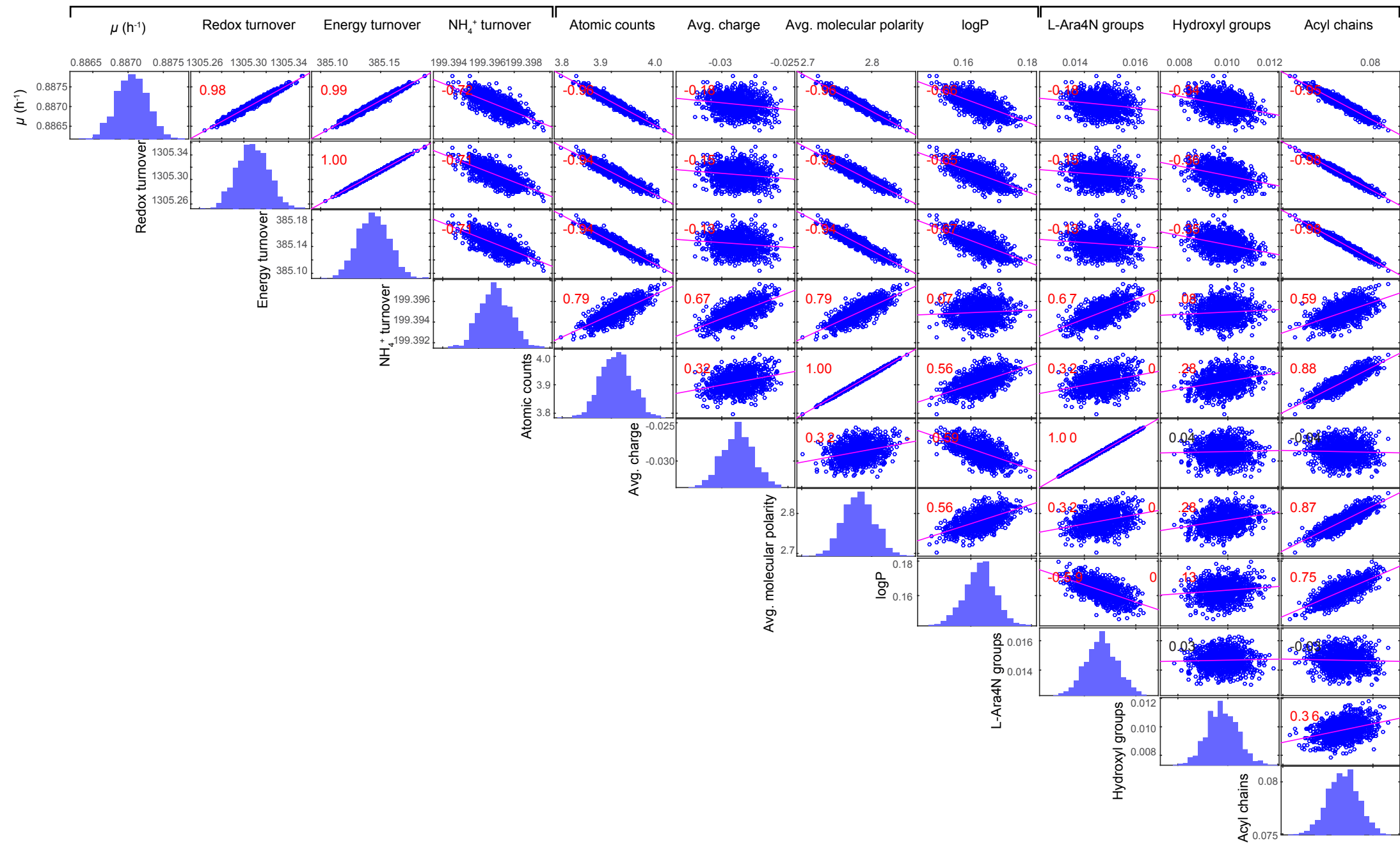


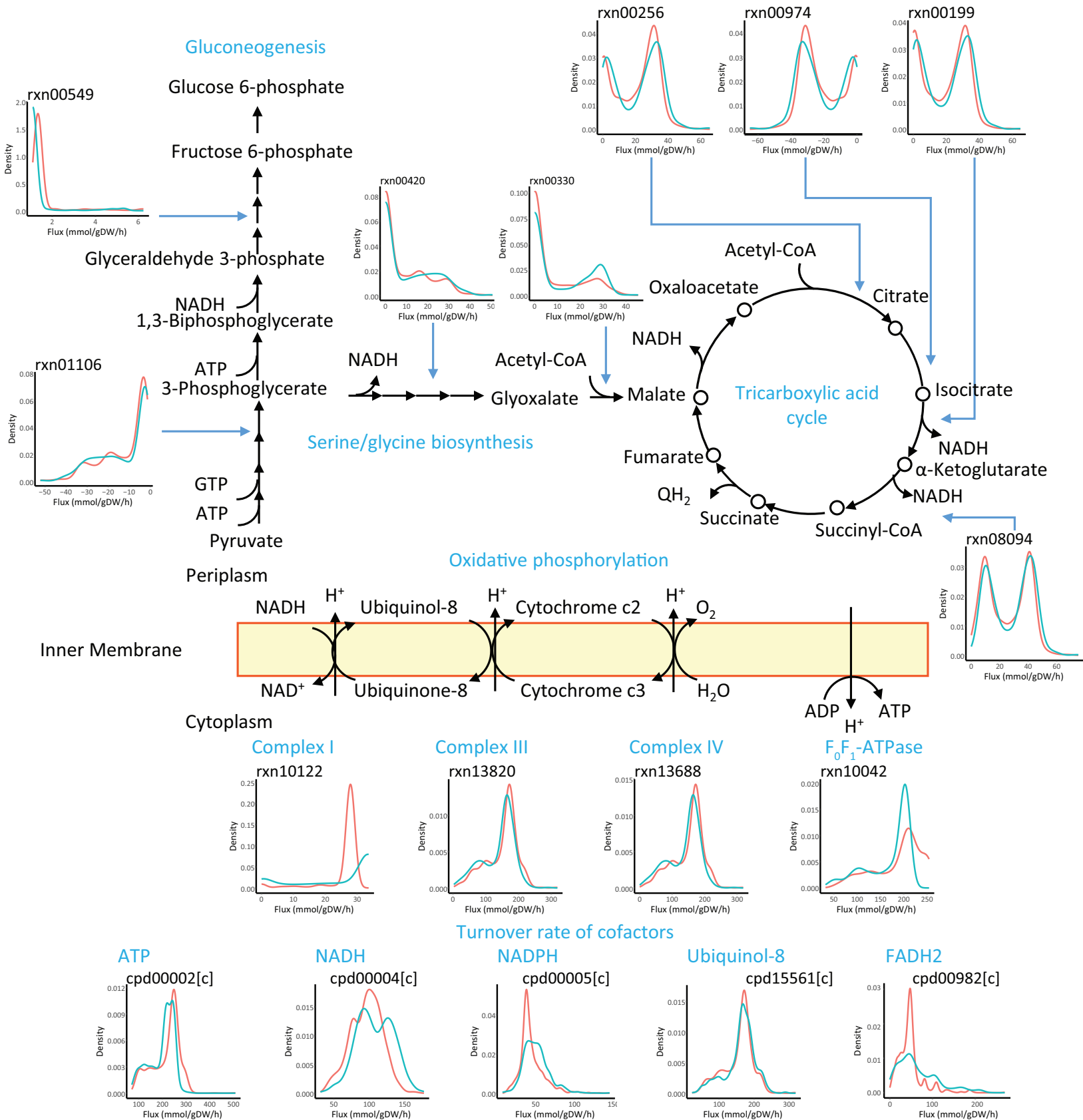





PM1 (Carbon)	Biolog /PAO1	PM2 (Carbon)	Biolog /PAO1	PM3 (Nitrogen)	Biolog /PAO1			
L-Arabinose	x	x	Chondroitin Sulfate C	x	x	Ammonia	v	v
N-Acetyl-D-Glucosamine	v	v	a-Cyclodextrin	x	x	Nitrite	v	v
D-Saccharic Acid	x	x	b-Cyclodextrin	x	x	Sodium Nitrate	v	v
Succinic Acid	v	v	g-Cyclodextrin	x	x	Urea	v	v
D-Galactose	x	x	Dextrin	x	x	Biuret	x	x
L-Aspartic Acid	v	v	Gelatin	x	x	L-Alanine	v	v
L-Proline	v	v	Glycogen	x	x	L-Arginine	v	v
D-Alanine	v	v	Inulin	x	x	L-Asparagine	v	v
D-Trehalose	x	v	Laminarin	x	x	L-Aspartic Acid	v	v
D-Mannose	x	x	Mannan	x	x	L-Cysteine	v	v
Dulcitol	x	x	Pectin	x	x	L-Glutamic Acid	v	v
D-Serine	x	v	N-Acetyl-D-Galactosamine	x	x	L-Glutamine	v	v
D-Sorbitol	x	x	N-Acetyl-Neuraminic Acid	x	x	Glycine	v	v
Glycerol	v	v	b-D-Allose	x	x	L-Histidine	v	v
L-Fucose	x	x	D-Amygdalin	x	x	L-Isoleucine	v	v
D-Glucuronic Acid	x	x	D-Arabinose	x	x	L-Leucine	v	v
D-Gluconic Acid	v	v	D-Arabitol	x	x	L-Lysine	v	v
D,L-a-Glycerol Phosphate	x	v	L-Arabitol	x	x	L-Methionine	v	v
D-Xylose	x	x	Arbutin	x	x	L-Phenylalanine	v	v
L-Lactic Acid	v	v	2-Deoxy-D-Ribose	x	x	L-Proline	v	v
Formic Acid	v	v	i-Erythritol	x	x	L-Serine	v	v
D-Mannitol	v	v	D-Fucose	x	x	L-Threonine	v	v
L-Glutamic Acid	v	v	3-0-b-D-Galacto-pyranosyl-D-Arabinose	x	x	L-Tryptophan	v	v
D-Glucose-6-Phosphate	x	v	Gentobiose	x	x	L-Tyrosine	v	v
D-Galactonic Acid-g-Lactone	x	x	L-Glucose	x	x	L-Valine	v	v
D,L-Malic Acid	v	v	Lactitol	x	x	D-Alanine	v	v
D-Ribose	v	v	D-Melezitose	x	x	D-Asparagine	v	v
Tween 20	v	x	Maltitol	x	x	D-Aspartic Acid	x	x
L-Rhamnose	x	x	a-Methyl-D-Galactoside	x	x	D-Glutamic Acid	v	v
D-Fructose	v	v	b-Methyl-D-Galactoside	x	x	D-Lysine	v	v
Acetic Acid	v	v	3-Methyl Glucose	x	x	D-Serine	v	v
D-(+)-Glucose	v	v	b-Methyl-D-Glucuronic Acid	x	x	D-Valine	v	v
Maltose	x	x	a-Methyl-D-Mannoside	x	x	L-Citrulline	v	v
D-Melibiose	x	x	b-Methyl-D-Xyloside	x	x	L-Homoserine	x	x
Thymidine	x	x	Palatinose	x	x	L-Ornithine	v	v
L-Asparagine	v	v	D-Raffinose	x	x	N-Acetyl-L-Glutamic Acid	v	v
D-Aspartic Acid	x	x	Salicin	x	x	N-Phthaloyl-L-Glutamic Acid	v	x
D-Glucosaminic Acid	x	x	Sedoheptulosan	x	x	L-Pyrogutamic Acid	v	v
1,2-Propanediol	v	v	L-Sorbose	x	x	Hydroxylamine	x	v
Tween 40	v	x	Stachyose	x	x	Methylamine	x	x
a-Keto-Gutaric Acid	v	v	D-Tagatose	x	x	N-Amylamine	x	x
a-Ketobutyric Acid	v	v	Turanose	x	x	N-Butylamine	x	x
a-Methyl-D-Galactoside	x	x	Xylitol	x	x	Ethylamine	x	x
a-D-Lactose	x	x	N-Acetyl-D-glucosaminitol	x	x	Ethanolamine	v	x
Lactulose	x	x	g-Amino Butyric Acid	v	v	Ethylenediamine	x	x
Sucrose	x	x	d-Amino Valeric Acid	v	v	Putrescine	v	v
Uridine	x	v	Butyric Acid	v	v	Agmatine	v	v
L-Glutamine	v	v	Capric Acid	x	v	Histamine	v	v
m-Tartaric Acid	x	x	Caproic Acid	v	v	b-Phenylethylamine	v	v
D-Glucose-1-Phosphate	x	v	Citraconic Acid	x	x	Tyramine	v	v
D-Fructose-6-Phosphate	x	x	Citramalic Acid	v	v	Acetamide	v	v
Tween 80	v	x	D-Glucosamine	x	x	Formamide	x	x
a-Hydroxy Glutaric Acid-g-Lactone	x	x	2-Hydroxybenzoic acid	x	x	Glucuronamide	v	v
D,L-a-Hydroxy-Butyric Acid	v	v	4-Hydroxy Benzoic Acid Sodium	v	v	D,L-Lactamide	v	v
b-Methyl-D-Glucoside	x	x	b-Hydroxy Butyric Acid	v	v	D-Glucosamine	x	x
Adonitol	x	x	g-Hydroxy Butyric Acid	x	v	D-Galactosamine	x	x
Maltotriose	x	x	2-Oxovaleric acid	x	x	D-Mannosamine	x	x
2'-Deoxy Adenosine	x	x	Itaconic Acid	v	v	N-Acetyl-D-Glucosamine	v	v
Adenosine	v	v	5-Keto-D-Gluconic Acid	x	x	N-Acetyl-D-Galactosamine	v	v
Glycyl-L-Aspartic Acid	x	v	D-Lactic Acid Methyl Ester	x	x	N-Acetyl-D-Mannosamine	x	x
Citric Acid	v	v	Malonic Acid	v	v	Adenine	v	v
m-Inositol	x	x	Melibionic Acid	x	x	Adenosine	v	v
D-Threonine	x	x	Oxalic Acid	x	x	Cytidine	v	v
Fumaric Acid	v	v	Oxalomalic Acid	x	x	Cytosine	v	v
Bromo Succinic Acid	v	x	Quinic Acid	v	v	Guanine	v	v
Propionic Acid	v	v	D-Ribono-1,4-Lactone	x	x	Guanosine	v	v
Mucic Acid	x	x	Sebacic Acid	x	x	Thymine	v	v
Glycolic Acid	x	x	Sorbic acid	v	v	Thymidine	x	x
Glyoxylic Acid	x	x	Succinamic Acid	v	v	Uracil	v	v
D-Cellobiose	x	x	D-Tartaric Acid	x	x	Uridine	v	v
Inosine	v	v	L-Tartaric Acid	x	x	Inosine	v	v
Glycyl-L-Glutamic Acid	x	v	Acetamide	x	v	Xanthine	v	v
Tricarballic Acid	x	x	L-Alaninamide	v	v	Xanthosine	v	v
L-Serine	v	v	N-Acetyl-L-Glutamic Acid	v	v	Uric Acid	v	v
L-Threonine	x	v	L-Arginine	v	v	Alloxan	v	x
L-Alanine	v	v	Glycine	v	v	Allantoin	v	v
Ala-Gly	x	v	L-Histidine	v	v	Parabanic Acid	v	x
Acetoacetic Acid	v	v	L-Homoserine	x	v	D,L-a-Amino-N-Butyric Acid	x	x
N-Acetyl-D-Mannosamine	x	x	Hydroxy-L-Proline	v	v	g-Amino Butyric Acid	v	v
Mono Methyl Succinate	v	v	L-Isoleucine	v	v	e-Amino-N-Caproic Acid	x	x
Methyl Pyruvate	v	x	L-Leucine	v	v	D,L-a-Amino- Caprylic Acid	x	x
D-Malic Acid	x	x	L-Lysine	x	v	d-Amino-N-Valeric Acid	v	v
L-Malic Acid	v	v	L-Methionine	x	v	a-Amino-N-Valeric Acid	v	x
Glycyl-L-Proline	v	v	L-Ornithine	v	v	Ala-Asp	v	v
p-Hydroxy Phenyl Acetic Acid	v	v	L-Phenylalanine	x	v	Ala-Gln	v	v
M-Hydroxy Phenyl Acetic Acid	x	x	L-Pyrogutamic Acid	v	v	Ala-Glu	v	v
Tyramine	v	v	L-Valine	x	v	Ala-Gly	v	v
D-Psicose	x	x	D,L-Carnitine	v	v	Ala-His	v	v
L-Lyxose	x	x	Sec-Butylamine	x	x	Ala-Leu	v	v
Glucuronamide	x	x	D,L-Octopamine	v	v	Ala-Thr	v	v
Pyruvic Acid	v	v	Putrescine	v	v	Gly-Asn	v	v
L-Galactonic Acid-g-Lactone	x	x	Dihydroxy Acetone	x	x	Gly-Gln	v	v
D-Galacturonic Acid	x	x	2,3-Butanediol	v	v	Gly-Glu	v	v
b-Phenylethylamine	x	x	Diacetyl	x	x	Gly-Met	x	v
2-Aminoethanol	v	v	3-Hydroxy 2-Butanone	x	x	Met-Ala	v	v

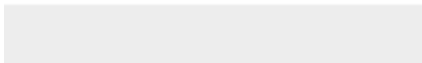
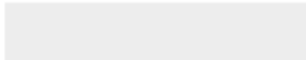
Figure 5


Specific growth and turnover rates (mmol-gDW-h⁻¹)Apparent properties of Lipid A (gDW⁻¹)[Click here to download Figure 5.pdf](#)



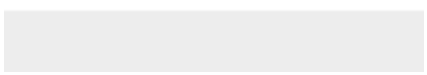
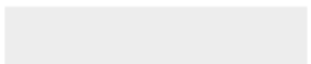


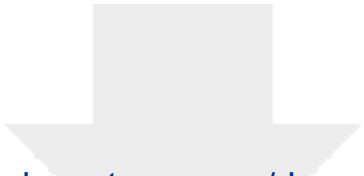
Click here to access/download
Supplementary Material
additionalFile1.docx







Click here to access/download
Supplementary Material
additionalFile2.xlsx






Click here to access/download
Supplementary Material
additionalFile3.xlsx

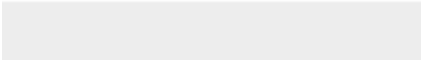



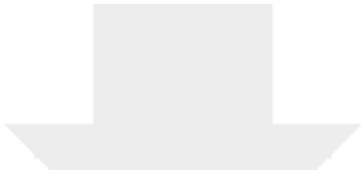


Click here to access/download
Supplementary Material
additionalFile4.xlsx




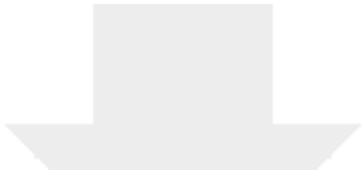
Click here to access/download
Supplementary Material
additionalFile5.xlsx






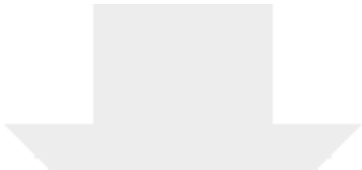
Click here to access/download
Supplementary Material
additionalFile6.xlsx







Click here to access/download
Supplementary Material
additionalFile7.xlsx



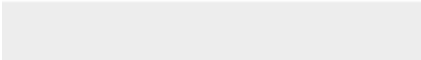



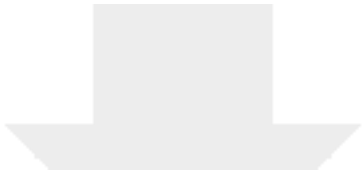
Click here to access/download
Supplementary Material
additionalFile8.xlsx






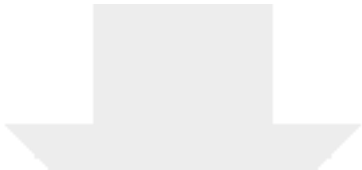
Click here to access/download
Supplementary Material
additionalFile9.xlsx






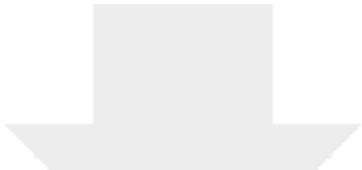
Click here to access/download
Supplementary Material
additionalFile10.xlsx







Click here to access/download
Supplementary Material
additionalFile11.xlsx



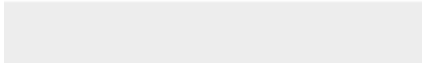



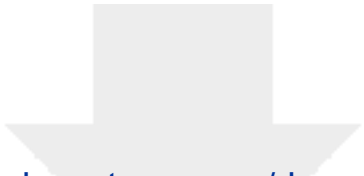
Click here to access/download
Supplementary Material
additionalFile12.xlsx






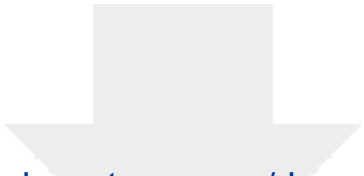
Click here to access/download
Supplementary Material
additionalFile13.xlsx






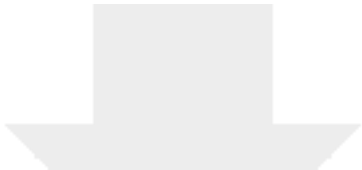
Click here to access/download
Supplementary Material
additionalFile14.xlsx






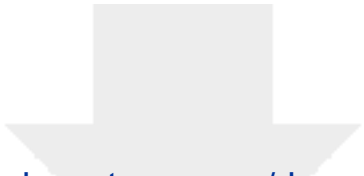
Click here to access/download
Supplementary Material
additionalFile15.xlsx







Click here to access/download
Supplementary Material
additionalFile16.xlsx



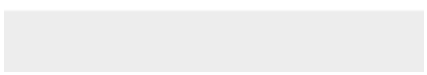
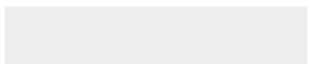



Click here to access/download
Supplementary Material
additionalFile17.xlsx



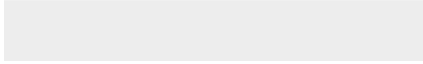



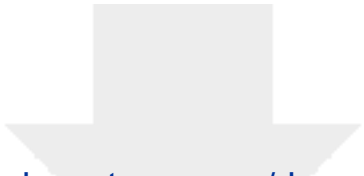
Click here to access/download
Supplementary Material
additionalFile18.xlsx






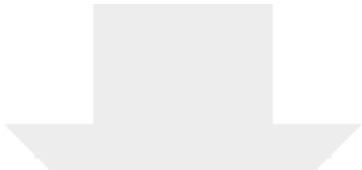
Click here to access/download
Supplementary Material
additionalFile19.xlsx






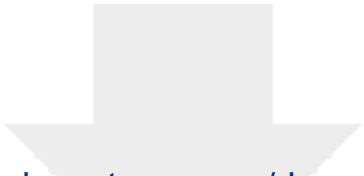
Click here to access/download
Supplementary Material
additionalFile20.xlsx







Click here to access/download
Supplementary Material
additionalFile21.xlsx



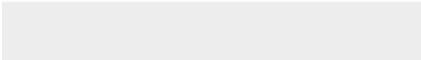



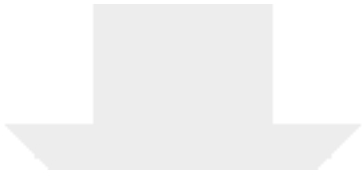
Click here to access/download
Supplementary Material
additionalFile22.xlsx






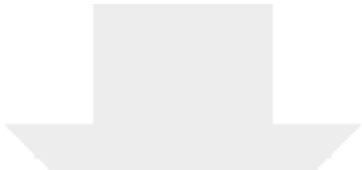
Click here to access/download
Supplementary Material
additionalFile23.xlsx







Click here to access/download
Supplementary Material
additionalFile24.xlsx



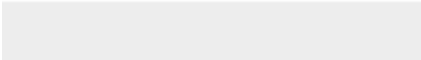



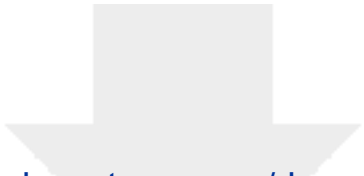
Click here to access/download
Supplementary Material
additionalFile25.xlsx






Click here to access/download
Supplementary Material
additionalFile26.xlsx





Click here to access/download
Supplementary Material
additionalFile27.xlsx





Professor Jian Li
Head, Laboratory of Antimicrobial Systems Pharmacology
Monash Biomedicine Discovery Institute

Dr Laurie Goodman
Editor-in-Chief
GigaScience

16 October 2017

Dear Dr Goodman,

We are pleased to submit our manuscript entitled “*Genome-scale metabolic modelling of responses to polymyxins in Pseudomonas aeruginosa*” for your consideration as an original Research Article in *GigaScience*.

Antimicrobial resistance has become one of the greatest threats to global health today. Multidrug-resistant (MDR) *P. aeruginosa* has been categorised by the World Health Organization as a “Critical” Gram-negative ‘superbug’ against which no new antibiotics will be available in the near future. Polymyxins are ‘old’ antibiotics firstly discovered in 1947, but have been abandoned since the 1970s. Over the last decade polymyxins have been revived as the last-line therapy against Gram-negative ‘superbugs’, including *P. aeruginosa*, which are resistant to all other antibiotics. However, the mechanism of their antibacterial activity remains largely unknown.

Here we report the construction of a superior genome-scale metabolic model (GSMM) *iPAO1* for *P. aeruginosa* PAO1 which represents *the largest genome-scale metabolic model thus far for any Gram-negative bacteria*. *iPAO1* provides a powerful systems pharmacology tool to elucidate the complex mode of action of antibiotics and shift the paradigm of the “one-gene, one-receptor, one-mechanism” approach. It is able to quantitatively simulate complex bacterial cellular responses in response to antibiotic treatments.

To date, there are four curated GSMMs for *P. aeruginosa*, iMO1056 (developed in 2008), Opt20896429 (2010), iMO1086 and iPae1146 (two minor updated versions of iMO1056 developed in 2011 and 2017, respectively), and all are for the strain PAO1. *Unfortunately, none of these four GSMMs incorporates the periplasmic space, and glycerolphospholipid (GPL) and lipopolysaccharide (LPS) biosynthesis is very poorly represented*. These shortcomings significantly limit their usefulness for antimicrobial pharmacology. Growth prediction with *iPAO1* on 190 carbon and 95 nitrogen nutrients outperformed all the previous models with an accuracy of 89.1%. Prediction of the essential genes for growth on rich media achieved a high accuracy of 87.9%. Specifically, the significant advantages of our *iPAO1* include: (1) incorporation of the periplasmic space; (2) addition of detailed GPL and LPS biosynthesis pathways supported by our own metabolomics and lipidomics data; and (3) significant expansion of the modelling scale with a high prediction accuracy. For the first time, metabolic simulation using *iPAO1* showed that lipid A modifications exert limited impacts on bacterial growth and metabolism, but remarkably change the physiochemical properties of bacterial outer membrane. Modelling with transcriptomics constraints revealed a broad range of metabolic responses to polymyxin treatment, including reduced biomass formation, upregulated amino acids catabolism, induced tricarboxylic acid cycle, and increased redox turnover. Overall,

Department of Microbiology
19 Innovation Walk
Monash University
VIC 3800, Australia
Telephone: (+61 3) 990 39702 Facsimile: (+61 3) 990 29222 Email: Jian.Li@monash.edu
Web: www.monash.edu/pharm/research/areas/drug-delivery/labs/li-lab

Unintended recipient: please notify as soon as possible and destroy all pages received



Professor Jian Li
Head, Laboratory of Antimicrobial Systems Pharmacology
Monash Biomedicine Discovery Institute

our GSMM approach has a significant potential in accelerating antimicrobial pharmacological discovery against Gram-negative 'superbugs'.

To the best of our knowledge, this study is the first to integrate antimicrobial pharmacology, computational biology, metabolic network and systems pharmacology to analyse large-scale datasets, in order to better understand the dynamic and complex nature of polymyxin killing and resistance. We believe this manuscript perfectly matches the theme of *GigaScience* and will be of broad interest to microbiologists, bioinformaticians and antimicrobial researchers.

We confirm that our submission comprises original and unpublished material which is not currently under consideration for publication elsewhere, and has been approved by all authors. Thank you for considering our work for publication in *GigaScience*. We look forward to your correspondence.

Yours sincerely,

A handwritten signature in blue ink, appearing to be 'Jian Li'.

Jian Li PhD

A handwritten signature in blue ink, appearing to be 'Falk Schreiber'.

Falk Schreiber PhD